K-matrix fits to $\pi N \to N\pi$ and $\pi N \to N\pi\pi$ in the resonance region $\sqrt{s} = 1.3$ to 2.0 GeV

R. S. Longacre,* T. Lasinski,† A. H. Rosenfeld, and G. Smadja‡
Department of Physics and Lawrence Berkeley Laboratory, University of California, Berkeley, California 94720

R. J. Cashmore§ and D. W. G. S. Leith
Stanford Linear Accelerator Center, Stanford University, Stanford, California 94305
(Received 28 October 1977)

Starting with partial-wave amplitudes for $\pi N \to N\pi$ and $\pi N \to$ several isobar-model states of $N\pi\pi$, we are able to apply the constraint of unitarity (using the K matrix). This permits the removal of the overall phase ambiguity of the isobar amplitudes at each energy. The K-matrix fits generate a smooth prescription for the T-matrix amplitudes, enabling us to search the complex energy plane for poles. The uniqueness of these poles is demonstrated by doing Breit-Wigner refits to the fitted T-matrix amplitudes. The success of the refits and the obvious interpretation justifies a simple determination of coupling signs for which there can be checks with theory.

I. INTRODUCTION

The various aspects of our partial-wave analysis of the reaction $\pi N \to N\pi\pi$ in the (1300–2000)-MeV region were recently presented in a series of publications.[1-5] The purpose of this report is to discuss in detail yet another aspect: the K-matrix formalism and the procedure of parametrization for the partial-wave amplitudes. To see how this topic fits into the whole scheme, it will be useful to review briefly the salient features of our analysis.

It is assumed that the reaction $\pi N \to N\pi\pi$ proceeds through several intermediate quasi-two-particle states. For the intermediate states, we specifically consider the isobars Δ, ρ, and ϵ with their mass-IJ^P quantum numbers as 1236-$\frac{3}{2}\,\frac{3}{2}^+$, 760-$11^-$, and 650-$00^+$. Restricting ourselves to orbital $L \leq 3$ and total $J \leq 7/2$, we construct the total amplitude T_{23} for $\pi N \to N\pi\pi$ as a linear sum of the amplitudes for production of each isobar, or, schematically,

$$T_{23} = aT_{\pi\Delta} + bT_{\rho N} + \cdots ,$$

where the coefficients contain the necessary kinematical factors, angular functions, Clebsch-Gordan coefficients, etc. Details of this isobar model, partial-wave expansions, and related topics are given in Ref. 1 which forms the basis of our analysis.

Equipped with this formalism and 200 000 events in the energy range 1.3 to 2.0 GeV for the three charge channels $\pi^+\pi^-n$, $\pi^-\pi^0p$, and $\pi^+\pi^0p$, we performed maximum-likelihood fits and found two solutions: solution A containing 24 partial waves, and solution B containing 28 partial waves. These were reported in Ref. 2 and the ambiguity between the two was resolved in Refs. 2 and 3. For details of the fitting program, tests, and quality of the solutions, etc. refer to Ref. 4.

From a group-theoretic point of view, one would like to think of the process $\pi N \to N\pi\pi$ as taking place through a single-particle metastable state or resonance. The complete picture then becomes $\pi N \to$ resonances $\to$ quasi-two-particle states $\to N\pi\pi$. An immediate point of interest in doing the entire partial-wave analysis is to find these resonant states, obtain their characteristic parameters, and make comparisons with predictions from symmetry groups and other theoretical models, particularly $SU(6)_W$. Such comparisons are made in Ref. 5.

The subject matter of the present paper which meets the three definite needs of the analysis are as follows:

First, the Argand amplitudes reported in Refs. 2–4 were obtained from an energy-independent analysis. This means that they were defined at discrete energies and lacked continuity from one energy to another. The methods to express them as smooth complex functions of the total energy W are now presented.

Second, the Argand amplitudes presented so far also have an arbitrary phase at each energy. In this paper we show how the constraints of unitarity and knowledge of elastic amplitudes can be utilized to remove this arbitrariness in phase.

Third, three possible ways are discussed to obtain the much desired resonance parameters.

The present paper is more detailed than the letter published earlier.[6] The K matrix is first introduced which is free from branch cuts in the total energy and is related to the T matrix in such a way as to satisfy the unitarity constraint imposed on the S matrix. This relation, an integral equation, is then reduced to a matrix equation by making simplifying assumptions concerning the subenergy dependence of the T- and K-matrix am-

plitudes. We also relate the new reduced amplitudes appearing in the matrix equation to the cross section. In Sec. III we discuss how the K matrix can be used to scale statistical errors and show how the overall arbitrary phase of the isobar-model amplitudes can be removed by the K matrix. The K matrix, suitably parametrized with real poles and background terms, is then fitted to the energy-independent Argand amplitudes by using the minimizing method due to Rosenbrock.[7] As a result of this fit, we obtain the resonance parameters for the K matrix, determine the arbitrary phase at each energy (all Argand diagrams are now determined to within an overall sign which is chosen conventionally; see Sec. IV), and obtain a smooth prescription for each amplitude. The results on χ^2 are given in Tables II and III and the Argand diagrams are displayed in Fig. 3. In Sec. V, our matrix equation is extended analytically into the complex W plane to determine the complex poles, their residues, and the partial widths for the T amplitudes. This constitutes another approach to extracting resonance parameters. A third approach (Sec. VI) is to do a refit of the smooth amplitudes from the K matrix fit using a unitary background plus a Breit-Wigner term. Results from these three methods are summarized in Table V. In Sec. VII, we give a prescription for fixing coupling signs for a resonance coupled to different channels. These signs are useful for comparison with theory. Finally, two other channels, $N\eta$ and $N\pi\pi\pi$, are predicted from our analysis and their evidence is discussed in Sec. VIII.

II. K-MATRIX FORMALISM

In this section we discuss how three-particle cross sections can be described in terms of the isobar-model amplitudes. We also discuss how an integral K-matrix equation can be reduced to an algebraic equation. Furthermore, we introduce the parametrization of our K matrix which is used to describe simultaneously $N\pi \to N\pi$ and $N\pi \to N\pi\pi$ partial-wave amplitudes.

The cross section for $2 \to 3$ particle processes in our normalization is[1]

$$\sigma=\frac{(2\pi)^6}{4F}\int |T_{23}|^2\delta^4\Big(P-\sum_i q_i\Big)\frac{1}{(2\pi)^4} \times \frac{d^3q_1}{2e_1}\frac{d^3q_2}{2e_2}\frac{d^3q_3}{2e_3}, \tag{2.1}$$

where P is the overall four-momentum and q_i is the four-momentum of the ith particle in the final state:

$$q_i=(e_i,\vec{q}_i). \tag{2.2}$$

F is the Møller invariant flux factor,

$$F=|Q_1|\sqrt{s}\ . \tag{2.3}$$

Here Q_1 is the center-of-mass (c.m.) momentum of the beam particle and $\sqrt{s}$ is the c.m. energy of the system. Finally T_{23} is the invariant matrix element for the $2 \to 3$ particle process.

Now, in the context of the isobar model, we assume that the reaction proceeds through three quasi-two-body channels,

$$\begin{aligned} &\pi N \to \pi\Delta(1236)\\ &\quad \to N\rho(760)\\ &\quad \to N\epsilon\ , \end{aligned} \tag{2.4}$$

where ϵ represents a strong S-wave $\pi\pi$ final-state interaction at around 650 MeV. Appendix F extends the formalism of Ref. 1 to give the total cross section in terms of the partial-wave amplitudes:

$$\sigma=\frac{\pi}{4Q_1\sqrt{s}}\sum_{J^P}(J+\tfrac{1}{2})\Big[\sum_n\int |T^{J^P}_{ln}(s_n,s)|^2\,\frac{Q_nq_nds_n}{4\sqrt{s}\,4\sqrt{s_n}}+\sum_n\sum_m\iint T^{J^P}_{lm}(s_m,s)\Phi^{J^P}_{mn}T^{J^P}_{lm}(s_m,s)ds_nds_m\Big]. \tag{2.5}$$

Here subscript l indicates the incoming partial wave; m and n denote the discrete set of quantum numbers necessary to describe the quasi-two-particle state in the angular momentum representation; Q_n is the momentum of the n-type isobar in the overall c.m.; q_n and s_n are the breakup momentum and the energy squared of the n-type isobar in its own rest frame. Finally, the functions Φ^{JP}_{mn} are the recoupling coefficients as given in Ref. 8. Notice that we have not yet integrated over the Dalitz-plot variables s_m and s_n in the second term on the right-hand side.

We have given the total cross section for two particles scattering into three particles via quasi-two-particle amplitudes of the isobar model. Using the K-matrix representation of Graves Morris[9] and Jacobson,[10] we can write an integral K-matrix equation for two-particle scattering. We extend this integral equation to quasi-two-particle systems by defining $T_{if}(p_{i\alpha},q_{f\beta})$, where i is the incoming state of up to three particles ($\alpha \leq 3$), f is the outgoing state of up to three particles ($\beta \leq 3$), and p,q are the four-momenta of the particles. This extension is accomplished by defining a K

matrix $K_{if}(p_{i_\alpha}, q_{f_\beta})$ which is related to the above T_{if} by an integral equation analogous to that for $2 \to 2$ scattering:

$$T_{if}(p_{i_\alpha}, q_{f_\beta}) - K_{if}(p_{i_\alpha}, q_{f_\beta}) = \frac{i}{2}\sum_{m'} \int \prod_{k=1}^{\sigma} \frac{d^3 p_k}{2\epsilon_k} T_{im'}(p_{i_\alpha}, p_{m'_\sigma}) K_{m'f}(p_{m'_\sigma}, q_{f_\beta}) \times \delta^4\left(P - \sum_j^{\sigma} p_j\right). \tag{2.6}$$

If $K_{if}(p_{i_\alpha}, q_{f_\beta})$ is Hermitian then $T_{if}(p_{i_\alpha}, q_{f_\beta})$ is unitary. This is shown in Appendix A after we make a partial-wave expansion via the isobar model.

If we expand T_{if} in terms of partial waves and use the isobar-model decomposition as we did above for the cross section, we obtain (γ = two-particle state, j, k = three-particle states, $i \to$ several n isobars, $f \to$ several m isobars for a given J^P state)

$$T^{J^P}_{nm} - K^{J^P}_{nm} = \frac{i}{2}\sum_{\gamma} T^{J^P}_{m\gamma} \frac{Q_\gamma}{4\sqrt{s}} K^{J^P}_{\gamma m} + \frac{i}{2}\sum_j \int \frac{T^{J^P}_{nj} Q_j q_j K^{J^P}_{jm}}{4\sqrt{s}\,4\sqrt{s_j}} ds_j + \frac{i}{2}\sum_j \sum_{j\neq k} \sum_k \int T^{J^P}_{nj} \Phi^{J^P}_{jk} K^{J^P}_{km} ds_j ds_k. \tag{2.7}$$

In Eq. (2.7) $K^{J^P}_{\gamma m}$ has direct two-particle channel cuts removed, while $K^{J^P}_{jm}$ has quasi-two-particle cuts of the three-particle channel removed (which in our model describes the three-particle system). It should be noted that $K^{J^P}_{jm}$ still has two-particle subenergy cuts present. If we include the stable two-body states and also the diagonal elements of the three-body state in $\Phi^{J^P}_{\gamma\lambda}$, we may rewrite Eq. (2.7) as

$$T^{J^P}_{nm} - K^{J^P}_{nm} = \frac{i}{2}\sum_{\gamma\lambda} \int T^{J^P}_{n\gamma} \Phi^{J^P}_{\gamma\lambda} K^{J^P}_{\lambda m} ds_\gamma ds_\lambda. \tag{2.8}$$

Now the functions $\Phi^{J^P}_{\gamma\lambda}$ have the significance

$$\Phi^{J^P}_{\gamma\lambda} = \frac{Q_\lambda}{4\sqrt{s}} \delta_{\gamma\lambda}\delta(s_\gamma - s)\delta(s - s_\lambda) \tag{2.9}$$

for the stable two-body states $|\gamma\rangle$ and $|\lambda\rangle$, and

$$\Phi^{J^P}_{\gamma\lambda} = \frac{Q_\lambda q_\lambda}{4\sqrt{s}\,4\sqrt{s_\lambda}} \delta_{\gamma\lambda}\delta(s_\gamma - s_\lambda) \tag{2.10}$$

for the quasi-two-body states $|\gamma\rangle$ and $|\lambda\rangle$ which belong to the same three-body angular momentum representation. (We call this the "diagonal element" of the three-body states and it is simply a statement of our normalization convention.) Henceforth we shall discuss a single partial wave, so the superscript J^P can be dropped.

As it stands, Eq. (2.8) is an integral equation. We shall now make certain factorization assumptions that will reduce Eq. (2.8) to a matrix equation. It is clear that a matrix equation will be easier for practical calculations (i.e., fitting the isobar amplitudes). Indeed the factorization assumptions we make are already inherent in the isobar model.

We assume $T_{\alpha\beta}$ to factor,

$$T_{\alpha\beta} = \tau_{\alpha\beta} f^*_\alpha f_\beta, \tag{2.11}$$

where f_α accounts for the barrier factors and final-state factors of the isobar decay and $\tau_{\alpha\beta}$ is only a function of s.

In addition, we assume that $K_{\alpha\beta}$ can be factored in the same way:

$$K_{\alpha\beta} = k_{\alpha\beta} f^*_\alpha f_\beta, \tag{2.12}$$

where k depends only on the total energy W and is free from branch points in the energy plane. We shall take it to be a real function of $s = W^2$. If the several final-state resonance bands did not overlap, then a real K matrix would imply a symmetric T matrix.

We can now reduce the integral Eq. (2.8) to a matrix equation by the substitution of $K_{\alpha\beta}$ and $T_{\alpha\beta}$:

$$\tau_{\alpha\beta} - k_{\alpha\beta} = \frac{i}{2}\sum_{\gamma\lambda} \tau_{\alpha\gamma}\Delta_{\gamma\lambda} k_{\gamma\beta}. \tag{2.13}$$

For stable two-body states

$$\Delta\gamma_\lambda = \frac{Q_\lambda \delta_{\gamma\lambda} |f_\gamma|^2}{4\sqrt{s}}, \tag{2.14}$$

i.e., diagonal with value proportional to Q times the barrier factor, and for three-body states

$$\Delta_{\gamma\lambda} = \int \Phi_{\gamma\lambda} f_\gamma f^*_\lambda ds_\gamma ds_\lambda. \tag{2.15}$$

The fact that the integrals over the subenergy variables can be evaluated separately to calculate $\Delta_{\gamma\lambda}$ imparts the desired matrix character to Eq. (2.13) which now connects a finite number of elements that depend on the total energy only. In Appendix A we demonstrate that Eq. (2.13) is consistent with the usual unitarity relation $\tau - \tau^+ = i\tau^+\Delta\tau$.

Next we discuss the barrier factor f. In general, we write

$$f_\alpha = W_\alpha B_\alpha(Q_\alpha, L_\alpha), \tag{2.16}$$

where B_α is the square root of the Blatt-Weisskopf barrier[11] which depends upon the orbital angular momentum in the center of mass. Our confidence in this choice for B_α has recently been increased by von Hippel and Quigg,[12] who showed that its validity is not restricted to square-well potentials and derived it from the general proper-

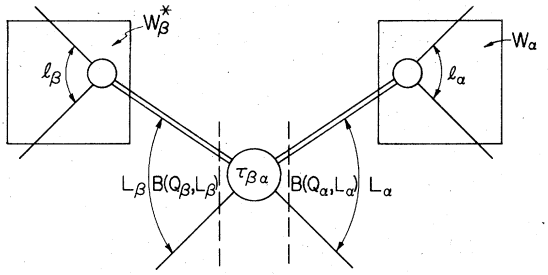

FIG. 1. s-channel diagram for isobar α outgoing and isobar β incoming, where $B(q,l)$ is square root of Blatt-Weisskopf (Ref. 11) barrier factor for momentum Q in an angular momentum state L. W_α is the Watson final-factor for the α isobar. W_β^* and W_α, see Eq. (2.17) in text.

ties of spherical harmonics.

We have introduced a weight factor W_α in Eq. (2.16) to take into account the essential characteristics of the isobar α. Thus, $W_\alpha = 1$ for the stable two-body state and is given by

$$W_\alpha = \frac{T_\alpha}{[\int |T_\alpha|^2 (q_\alpha/4\sqrt{s_\alpha}) ds_\alpha]^{1/2}} \tag{2.17}$$

for a quasi-two-body state involving the α isobar. Here T_α, not to be confused with the previous $T_{\alpha\beta}$, is defined as

$$T_\alpha = \frac{\gamma_\alpha B_\alpha(q_\alpha, l_\alpha)}{E_{r_\alpha} - \sqrt{s_\alpha} - i\gamma_\alpha q_\alpha B_\alpha^2(q_\alpha, l_\alpha)} . \tag{2.18}$$

In Fig. 1 we show the various elements that enter into the transition amplitude for β isobar $\to \alpha$ isobar. The quantities E_{r_α} and γ_α for the Δ, ρ, and ϵ isobars are listed in Table I. Substitution of Eqs. (2.17) and (2.18) into Eq. (2.16) yields

$$f_\alpha = \frac{T_\alpha(s_\alpha) B_\alpha(q_\alpha, L_\alpha)}{[\int |T_\alpha|^2 (q_\alpha/4\sqrt{s_\alpha}) ds_\alpha]^{1/2}} , \tag{2.19}$$

where Eq. (2.15) for the diagonal element $\Delta_{\alpha\alpha}$ representing the α isobar becomes

$$\Delta_{\alpha\alpha} = \frac{\int |T_\alpha|^2 B_\alpha^2 (Q_\alpha/4\sqrt{s})(q_\alpha/4\sqrt{s_\alpha}) ds_\alpha}{\int |T_\alpha|^2 (q_\alpha/4\sqrt{s_\alpha}) ds_\alpha} . \tag{2.20}$$

We see that the normalization in Eq. (2.17) was chosen so that $\Delta_{\alpha\alpha}$ is essentially an average of $Q_\alpha B_\alpha^2/(4\sqrt{s})$, which is a dimensionless quantity. Therefore $k_{\alpha\beta}$ in Eq. (2.13) is a dimensionless number, and in fact the whole Eq. (2.13) is dimensionless.

We assume that $k_{\alpha\beta}$ is real with no branch points and can be described by simple factorizable points (which represent the formation of N^* resonances) plus nonfactorizable background terms which are polynomials in $\sqrt{s}$. The K-matrix program KANAL which was written to do the fits had a possibility for three regular poles and a background linear in W, that is,

$$k_{\alpha\beta} = \sum_{r=1}^{3} \frac{\gamma_\alpha^r \gamma_\beta^r}{E_{r_\alpha} - W} + C_{\alpha\beta} + W B_{\alpha\beta} . \tag{2.21}$$

Turning our attention back to the cross section, we note that it can be expressed in terms of the reduced amplitudes τ_{1n}. Starting with Eq. (2.5) and taking only one partial wave and isobar, we obtain ($\sqrt{s_n} \equiv E_n$)

$$\sigma_{1n}(W) = \frac{\pi}{4Q_1 W} (J + \tfrac{1}{2}) \int |T_{1n}(W, E_n)|^2 \frac{Q_n q_n dE_n}{8W} . \tag{2.22}$$

By substitution of Eqs. (2.11) and (2.19) into Eq. (2.22), we get

$$\sigma_{1n}(W) = \frac{\pi}{16 Q_1 W^2} (J + \tfrac{1}{2}) \times \frac{\int |\tau_{1n}(W)|^2 \tfrac{1}{2} (Q_n q_n) B_1^2 B_n^2 |T_n(E_n)|^2 dE_n}{\int |T_n(E_n)|^2 \tfrac{1}{2} q_n dE_n} . \tag{2.23}$$

Noting that $\tau_{1n}(W)$ and B_1^2 are independent of E_n, this becomes

$$\sigma_{1n} = \frac{\pi}{Q_1^2} (J + \tfrac{1}{2}) |\tau_{1n}(W)|^2 \Delta_{11} \Delta_{nn} . \tag{2.24}$$

If the partial-wave S matrix is defined by

$$S_{\alpha\beta} = \delta_{\alpha\beta} + 2iA_{\alpha\beta} , \tag{2.25}$$

the cross section is given by

$$\sigma_{1n} = \frac{4\pi(J + \tfrac{1}{2}) |A_{1n}|^2}{Q_1^2} . \tag{2.26}$$

Comparing Eqs. (2.24) and (2.26), we have

TABLE I. Breit-Wigner parameters used in Watson final-state factors, Eq. (2.18).

Isobar, α	Mass, Er_α (pion masses)	Width, γ_α (dimensionless)	Orbital angular momentum, l_α
Δ	8.83	0.40	1
ρ	5.464	0.20	1
ϵ	6.0	0.8	0

$$A_{1n} = \frac{\sqrt{\Delta_{11}}\sqrt{\Delta_{nn}}\,T_{1n}}{2} . \quad (2.27)$$

The A_{1n} amplitudes are the results of the isobar-model fit to $\pi N - \pi\pi N$ (Refs. 2–4) and the A_{11} amplitudes come from the elastic phase-shift analysis EPSA.[13,14] The program KANAL was written to fit the A's by a χ^2 method, using the K-matrix parametrization of Eq. (2.21).

Before leaving the K-matrix formalism, we indicate how we dealt with the fact that there are two Δ isobars in the $N\pi\pi$ final state ($N\pi_1\pi_2 = \Delta_1\pi_2 + \Delta_2\pi_1$). We treated them as separate channels with the same coupling. This coupling was $\gamma_\Delta/\sqrt{2}$, where γ_Δ is the total Δ coupling. Once we calculated the T's for the individual Δ's, we added the amplitudes together as

$$T_\Delta = \frac{T_{\Delta 1}}{\sqrt{2}} + \frac{T_{\Delta 2}}{\sqrt{2}} . \quad (2.28)$$

An explanation of this equation and the last paragraph is found in Appendix G.

III. DETERMINATION OF THE OVERALL PHASE AND SCALING OF ERRORS

In this section we discuss how we use the K matrix to scale our statistical errors to more reasonable values. We also show how the intrinsic overall arbitrary phase of our isobar-model amplitudes at a given energy can be removed by the K matrix.

A. Scaling of errors

In order to use the K matrix, we needed to supplement our $N\pi\pi$ amplitudes A_{1n} with the elastic amplitudes A_{11}. Two sets of A_{11} were available, one from CERN[13] and another from Saclay.[14] Using these, we made two separate fits. However, it is well known that the deviations between the two solutions are greater than the statistical errors; this situation resulted in our use of larger errors in these fits. The errors, $\delta(A_{11})$, were calculated by taking the rms (root mean square) deviation between the two A_{11} solutions. For a few waves at some energies this external error was too small, so the statistical error claimed by Saclay analysis was used (no statistical error is quoted by CERN). For the inelastic waves it would be nice to use external errors. However, using our statistical errors which we felt were too small, we decided to scale our errors so that the inelastic and elastic data would contribute equally to the overall multichannel χ^2. For the purpose of scaling errors, we wanted to select a wave (or waves) that had one clear resonance in the elastic phase shift and where our inelastic fit would be in good agreement with the elastic phase-shift prediction. Resonances in the 1500-MeV region were not good candidates because we were missing inelastic data from 1540–1650 MeV.[15] Resonances near 1900 MeV were also poor candidates, since we had limited ourselves to F waves in our analysis. This meant we were unable to describe satisfactorily the peripheral production of pions that becomes important in this energy region.[4] For these reasons, the 1700-MeV resonance region seemed ideal. In this region there are four resonances that are clearly seen in the EPSA: the $S31$, $D33$, $D15$, and $F15$. Since $S31$ and $D33$ resonate near 1650, they could not be used because of the energy gap. The $D15$ is not in as good an agreement with the EPSA as the $F15$. Therefore, we only took the $F15$ wave to scale χ^2 elastic with χ^2 inelastic in our K-matrix fits.

The procedure was to adjust the errors on the inelastic amplitudes for the $F15$ until the χ^2 per energy bin was equal for the elastic and the inelastic contributions. We used only one pole and a constant background as parameters in the K-matrix fit for the $F15$ partial wave in the energy region 1585–1810 MeV with the inelastic amplitudes having one free phase at each energy. Notice that at this point we are using the K matrix to describe only the moduli of the inelastic amplitudes.

When we first fitted with external errors on the elastic and raw statistical errors on the inelastic, by far the greatest contribution to χ^2 came from the inelastic channels. As we scaled up the statistical errors on the inelastic amplitudes, the χ^2 began to shift to the elastic channel. At a scaling of three on the inelastic errors, the χ^2 per bin of energy became equal for the elastic and inelastic contributions. Three seems like a large factor. However, if one looks at the statistical errors quoted by Bareyre at Batavia[14] and compares them with the external errors, one also finds a factor of from 2 to 4. So for the rest of the partial-wave fits, we used three times the statistical errors for the inelastic and the external errors for the elastic amplitudes.

B. Overall phase

At each energy all the inelastic amplitudes are well determined with respect to each other but have an overall arbitrary phase. With the unitary constraint relating the elastic amplitudes to the inelastic amplitudes, we are now in a position to determine this phase at each energy. For this purpose we only consider dominant partial waves shown in Fig. 2. In particular, the $D15$ and the $F15$ which dominate partial waves in the energy range 1585–1810 MeV show good resonant motion

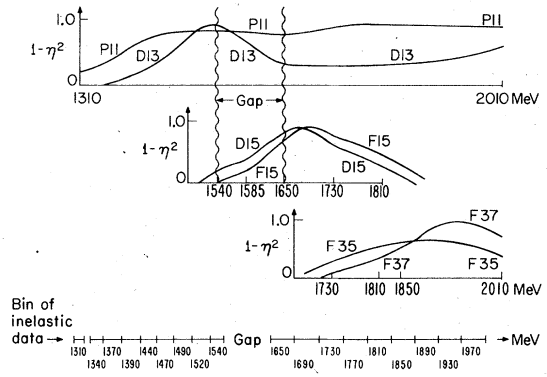

FIG. 2. Diagram of $1-\eta^2$ for the six different resonances used in determining the overall phase.

in the elastic channel; so we expect to see this behavior in the inelastic channel as well. This was our starting point for determination of the overall arbitrary phases in this energy region.

Our fitting program (KANAL) was designed to fit with an unknown overall phase ϕ_i at the ith energy bin for the inelastic data. First we obtained a solution for $F15$ and $D15$ from 1585–1810 MeV (8 elastic + 5 inelastic bins). Here we used a single pole and a constant background as parameters with an overall undetermined phase at each energy. This fit was performed separately for both the CERN and Saclay EPSA solutions for the elastic channel and resulted in four sets of overall phases, one set of five phases each for $D15$ and $F15$ waves. Our aim was to reduce these four different sets to only one set that would equally well describe the data for different inputs: $D15$(CERN), $D15$(Saclay), $F15$(CERN) and $F15$(Saclay). We accomplished this goal through an iterative process. The values of ϕ_i were essentially adjusted by hand until we obtained the best overall χ^2 for the four solutions. For minimizing the total χ^2 for solution A, however, a more complicated procedure given in Ref. 16 was used.

Next we looked at the $F35$ and $F37$ waves which went from 1730–1970 MeV in energy. In the overlap region (1730–1810 MeV), we minimized all four waves, each with two combinations, leaving the (1850–1970)-MeV phases free for the $F35$ and $F37$. However, this procedure did not change the overlap phases very much from the values obtained by just considering $D15$ and $F15$.

After finally arriving at a set of phases from 1650–1810 MeV, we determined the phases from 1850–1970 MeV just using $F35$ and $F37$, where one pole and constant background were again used in the K matrix. Thus, we were able to arrive at nine phases for our nine upper energies.

We then turned to the lower energies from 1310–1540 MeV. In this region the $D13$ and $P11$ are dominant waves and are ideal for determining the phases. The problem here, however, was to find a solution that would continue across the energy gap. The $D13$ at 1540 MeV is very inelastic, but at around 1650 MeV this is no longer the case. On the other hand, the $P11$ stays very inelastic all the way through the energy region. For this reason the $P11$ was the only partial wave that could be used to make the connection across the gap. Once we continue across the gap we may use, as above, both $D13$ and $P11$ to determine phases below the gap.

With the upper energy phases fixed on the values determined above, we parametrized the K matrix by two poles and a constant plus linear background. The pole positions in the K matrix were initially

TABLE II. Results of K matrix for solutions A and B.

	Solution A					Solution B				
Wave	χ^2 CERN	χ^2 Saclay	Degree of freedom	CERN χ^2/d.f.	Saclay χ^2/d.f.	χ^2 CERN	χ^2 Saclay	Degree of freedom	CERN χ^2/d.f.	Saclay χ^2/d.f.
$S11$	89	57	62	1.435	0.99	203	157	106	1.915	1.481
$S31$	136	142	73	1.863	1.945	114	125	82	1.390	1.524
$P11$	153	161	98	1.561	1.643	190	187	119	1.597	1.571
$P13$	118	89	47	2.511	1.894	197	172	55	3.582	3.127
$P33$						110	104	52	2.115	2.000
$D13$	202	225	142	1.423	1.585	221	210	148	1.493	1.419
$D33$	110	119	52	2.115	2.288	168	166	124	1.355	1.339
$D15$	59	70	20	2.950	3.500	65	81	20	3.250	4.050
$F15$	44	31	31	1.419	1.000	78	59	35	2.229	1.686
$F35$	27	21	34	0.794	0.618	40	34	34	1.176	1.000
$F37$	23	10	23	1.000	0.435	52	39	25	2.080	1.560
Total	961	925	582	1.651	1.589	1438	1334	800	1.797	1.667

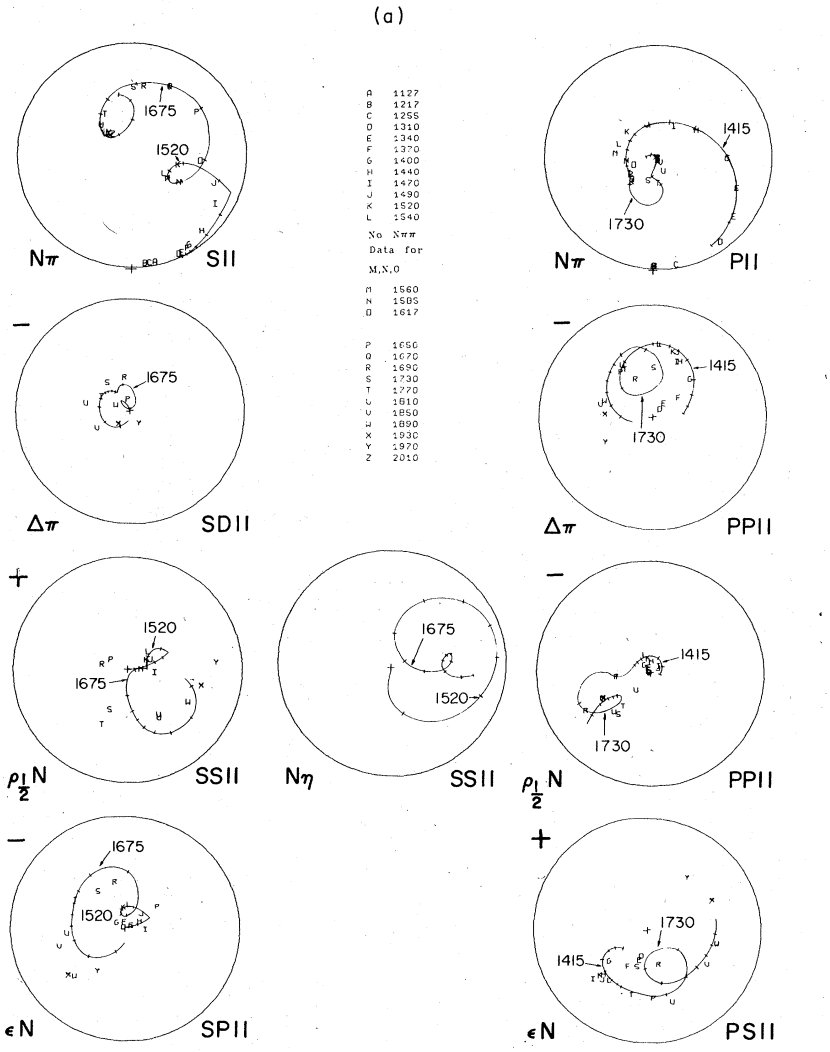

FIG. 3. *Continued*

set and held at 1415 and 1730 MeV (nominal positions of $P11$ resonances[14]), and the lower phases were left free to vary. We fitted over the entire energy range from 1370–2010 MeV in order to continue across the gap. This gave the $P11$ given in this paper. We later let the pole positions in the K matrix vary.

Having provided a continuation across the gap, we turned to the $D13$ solution which was also fitted in the same range (1310–2010 MeV) as the $P11$. For the $D13$ we used two poles and a constant and linear background. At this point the lower phases were determined with essentially the same procedure as was used for the upper energies.

IV. *K*-MATRIX FITS

In this section we give the results of the K-matrix fits. These fits were performed using the minimizing method due to Rosenbrock.[7] In Table II we give the χ^2, degree of freedom, and χ^2 per degree of freedom for each wave appearing in solutions A and B. Since the fits for the two solutions were done with different sets of waves and energy range, we present in Table III the χ^2 calculated over the same energy range and same number of waves. In Fig. 3 we display the Argand diagrams for solution B (Saclay) for the inelastic as well as the elastic channels. For solution A

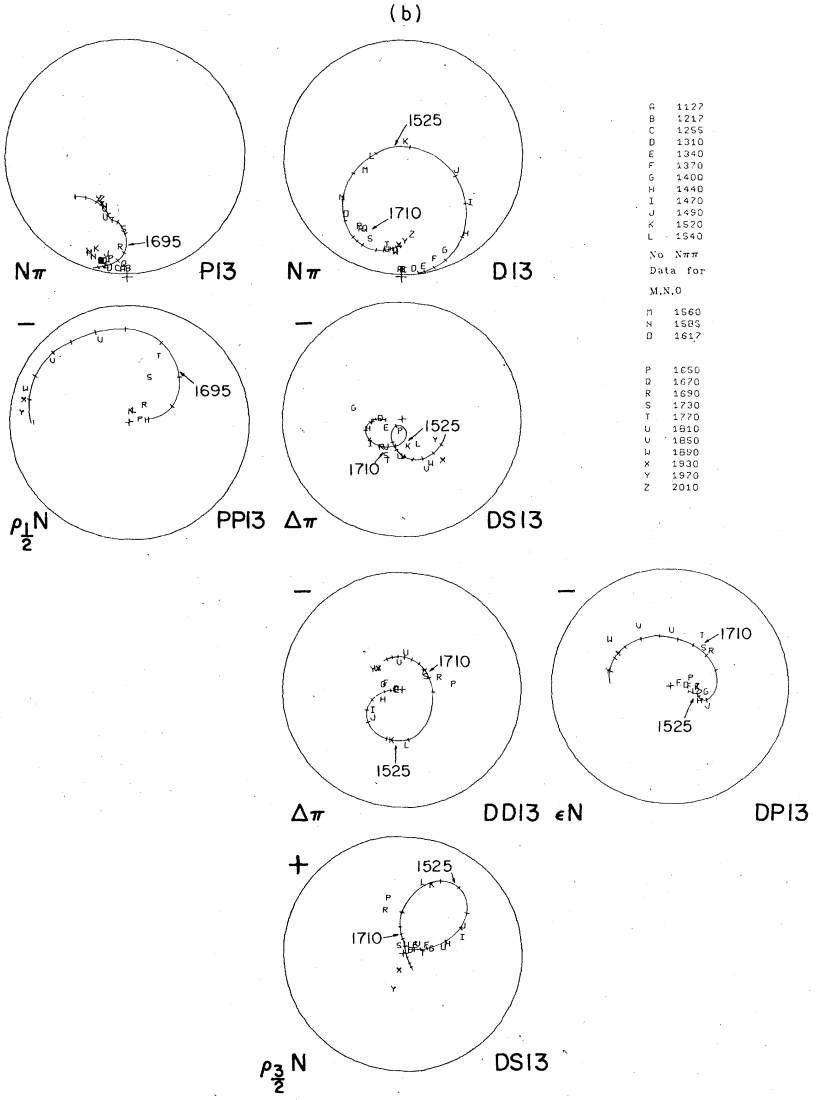

FIG. 3. *Continued*

TABLE III. K-matrix χ^2 solutions A and B over same energy range and same number of waves.

Wave	A χ^2 CERN	B χ^2 CERN	A χ^2 Saclay	B χ^2 Saclay
$S11$	89	114	57	86
$S31$	136	78	142	88
$P11$	153	152	161	148
$P13$	118	197	89	172
$D13$	202	221	225	210
$D33$	110	68	119	65
$D15$	59	65	70	81
$F15$	44	71	31	54
$F35$	27	40	21	34
$F37$	23	52	10	39
Total	961	1058	925	977

see Longacre's thesis.[16] The K-matrix pole positions and partial widths are shown in Table IV which also lists the T-matrix resonance parameters discussed in the next section. For an explanation of the signs attributed to the Argand diagrams (Fig. 3) and couplings (Table IV) see Sec. VII.

V. POLES IN THE T MATRIX

Now we discuss how Eqs. (2.13) and (2.20) are analytically continued into the complex energy plane. This continuation naturally leads to an analytic T matrix except for complex branch points associated with the isobars and poles due to s-channel resonances.

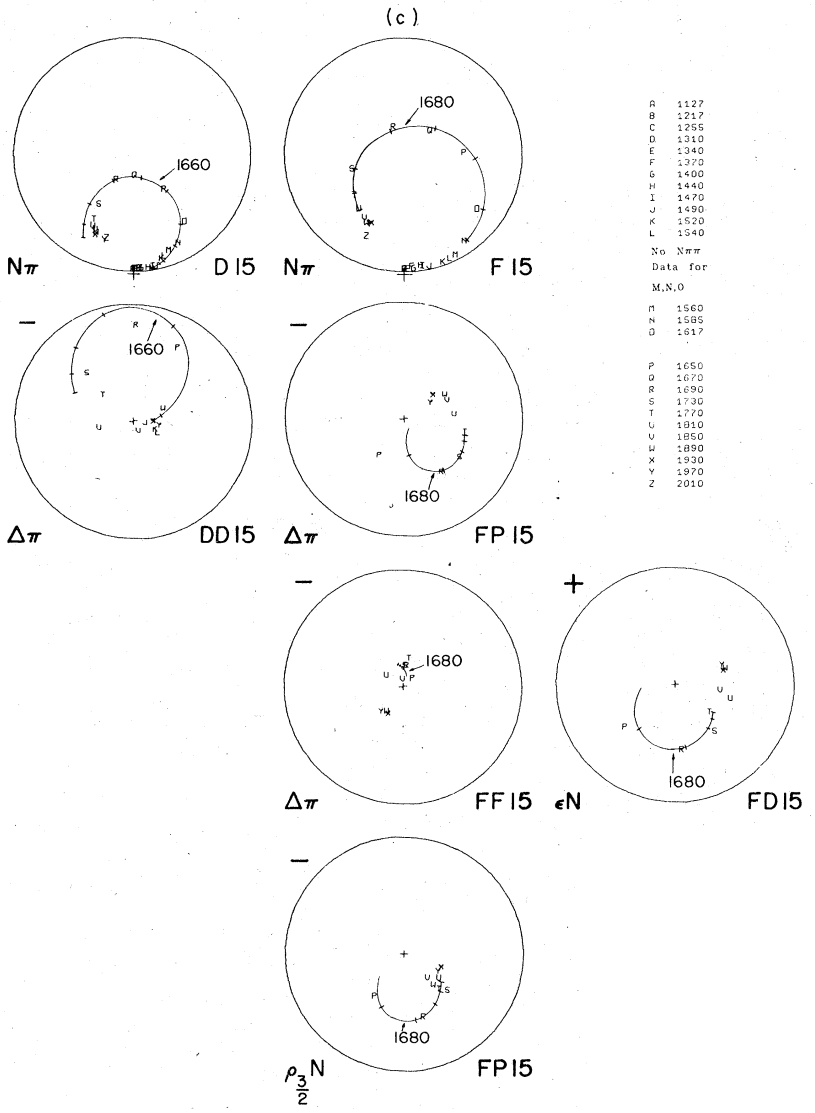

FIG. 3. *Continued*

A. Kinematics

Once the K-matrix fits were completed, we searched in the complex energy plane for poles identified with the different resonance states. Because the K matrix generates simple poles in the T matrix, the residue of the pole is factorizable. A simple proof of this is given in Appendix B. The residue matrix of the T-matrix pole is identified with the coupling of the resonant state to the different channels. One would like to relate this coupling matrix with the usual partial widths Γ of the resonance. The partial width is equal to the coupling times a kinematic factor. The question is: Should this kinematic factor be evaluated at the pole or on the real axis? We decided to take the kinematics calculated on the real axis because for a simple Breit-Wigner form with narrow width, the partial width will be more real and the sum of the partial widths will be closer to the total width. See Appendix C.

B. Analytic continuation

In order to search the complex energy plane for poles, we had to continue analytically the Δ_{mn} matrix into the complex plane. The off-diagonal terms of the Δ_{mn} matrix turn out to be from 5 to 20% of the diagonal elements. In view of the fact that these terms add little to the analytic sheet structure and a lot to the computer time, we set the off-diagonal terms of the Δ_{mn} matrix to zero when we searched for complex poles.

Now to continue the Δ_{mn} matrix to complex en-

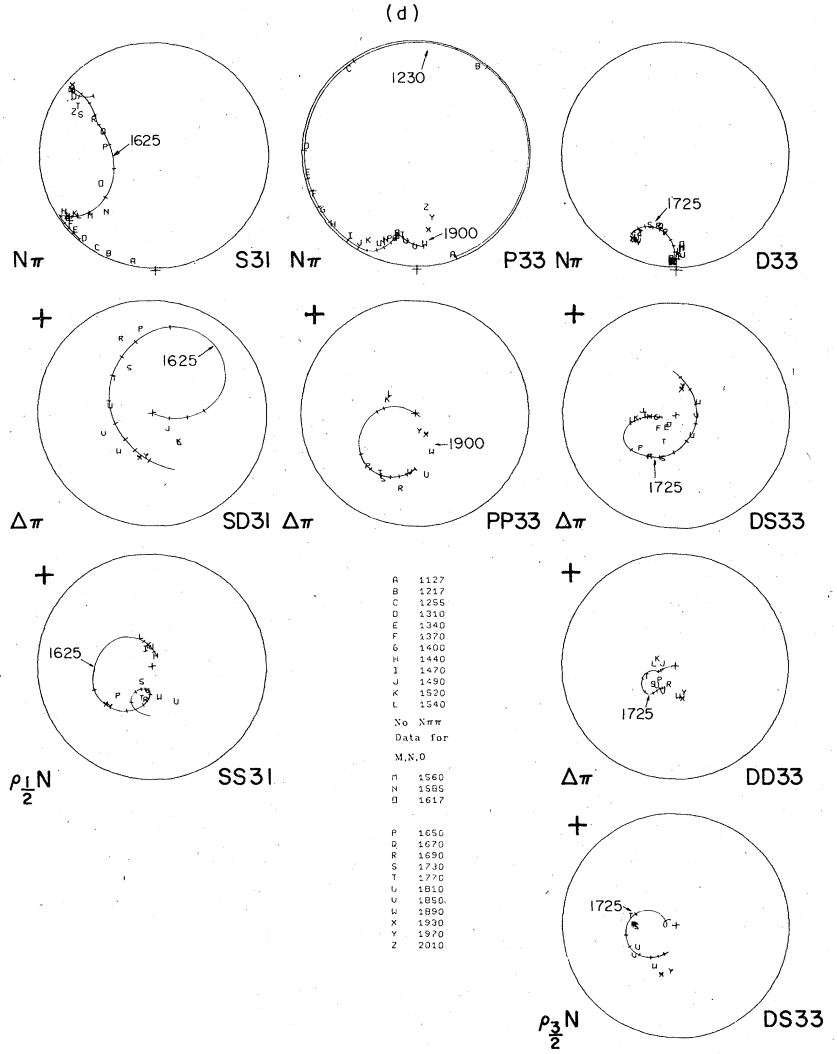

FIG. 3. *Continued*

ergy W, we have to do a contour integration in the complex diparticle mass E_α plane related to a given isobar. Let us rewrite Eq. (2.20) making the energy dependence explicit (in the remainder of this paper we shall sometimes set $E_\alpha = E$ for brevity:

$$\Delta = \frac{(1/4W)\int_{m_1+m_2}^{W-m_3} |T(E)|^2 Q(W,E) \tfrac{1}{2} q(E) B^2(W,E) dE}{\int_{m_1+m_2}^{W-m_3} |T(E)|^2 \tfrac{1}{2} q(E) dE} . \tag{5.1}$$

When we are on the real axis, all terms in the integral are real. Since we want all terms to be analytic in E_α, we must be able to expand them in a Taylor series with real coefficients as a function of E_α. Every term in the integral is obviously analytic except $|T_\alpha|^2$. However, we know that T_α is analytic. In fact, T_α can be related to a function m_α, which is free from cuts, by

$$T_\alpha = \frac{1}{m_\alpha - i q_\alpha} . \tag{5.2}$$

Recall that T_α is essentially the $2 \to 2$ scattering amplitude, so that m_α is an inverse K matrix. Therefore, $|T_\alpha|^2$ can be written as

$$|T_\alpha|^2 = \frac{1}{m_\alpha^2 + q_\alpha^2} , \tag{5.3}$$

which is obviously analytic.

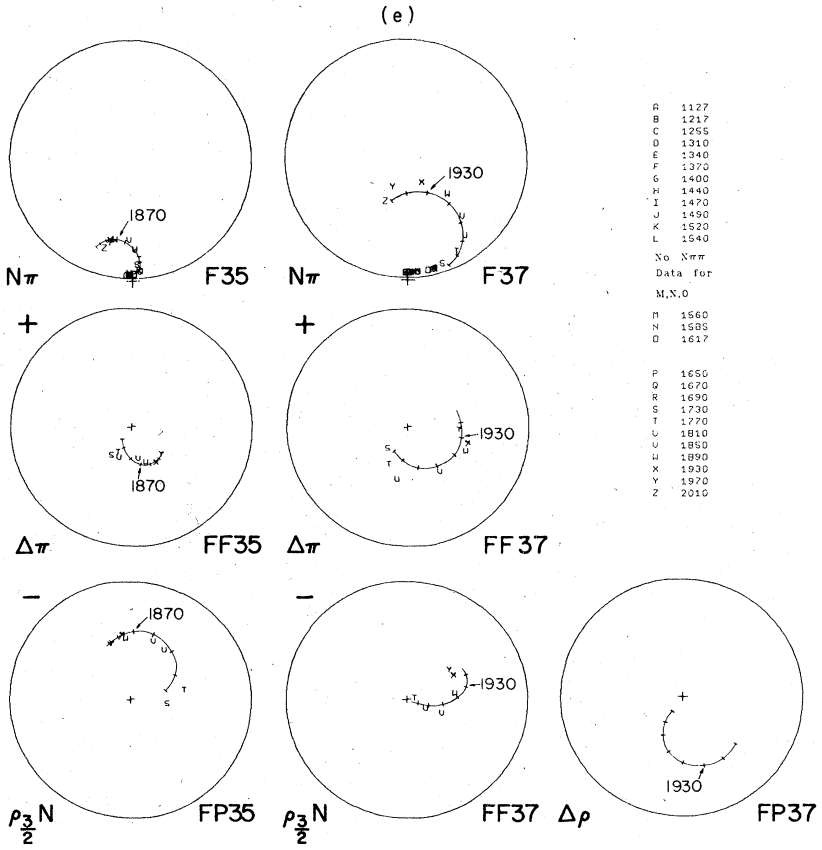

FIG. 3. Argand diagrams for the elastic and inelastic channels. The smooth curve on the Argand diagrams is the amplitude obtained from the K matrix when the description was possible. Cross-hatched marks on the curve correspond to the energies D, E, F, etc. The arrows indicate the known resonances of Ref. 14. The sign in the upper left-hand corner of each Argand plot converts amplitude to "baryon-first" convention.

1. The pole in $|T_\alpha|^2$

Next we derive Eq. (5.6) to show that $|T_\alpha|^2$ has a pole, and that it occurs exactly where the sheet-II pole occurs for the amplitude T_α of Eq. (5.2). We use the standard definition of sheets; the imaginary part of $q_\alpha > 0$ (<0) corresponds to sheet I (II). Therefore, dropping the α index, we have the usual relationships:

$$T_{\rm I}(E) = \frac{1}{m(E) - iq_{\rm I}(E)}\,,$$

$$T_{\rm II}(E) = \frac{1}{m(E) - iq_{\rm II}(E)} \tag{5.4}$$

$$m^*(E^*) = m(E), \quad q_{\rm I}(E) = -q_{\rm I}^*(E^*)\,,$$

$$q_{\rm I}(E) = -q_{\rm II}(E), \quad q_{\rm II}(E) = -q_{\rm II}^*(E^*)\,.$$

From Eqs. (5.3) and (5.4), we have

$$|T|^2 = \frac{1}{m^2(E) + q_{\rm I}^{\,2}(E)} = \frac{1}{m^2(E) + q_{\rm II}^{\,2}(E)}\,. \tag{5.5}$$

This can be written in a symmetric form using both sheets:

$$\begin{aligned} |T|^2 &= \frac{1}{m(E) - iq_{\rm I}(E)}\,\frac{1}{m^*(E^*) + iq_{\rm II}^*(E^*)} \\ &= T_{\rm I}(E)\,T_{\rm II}^*(E^*) \\ &= \frac{1}{m(E) - iq_{\rm II}(E)}\,\frac{1}{m^*(E^*) + iq_{\rm II}^*(E^*)} \\ &= T_{\rm II}(E)T_{\rm I}^*(E^*)\,. \end{aligned} \tag{5.6}$$

Since $T(E)$ is the two-body elastic scattering amplitude of the particles that make up the isobar, it will have a pole on sheet II that is properly identified with the isobar, as we set out to show.

2. Contours of integration

Notice that both integrals in Eq. (5.1) are path dependent because of the pole in $|T_\alpha|^2$. We can choose from among many paths of integration. We are, however, only interested in the paths that go most directly to the end points of integration because they lie near the physical region, which is just the real axis.

TABLE IV. K-matrix and T-matrix poles and partial Γ in MeV for both CERN and Saclay EPSA. The Γ are calculated from both the K-matrix samplings (real) and the T-matrix residues (complex) times the kinematics on the real axis at the pole. The sign superscripted to the partial width is explained in Sec. VII, and the T-matrix entries correspond to Method III of our paper in Phys. Lett. (Ref. 6). The K-matrix parameters are so unphysical that they were not even tabulated in Ref. 6.

Origin		Mass		Γ(total)		Γ(Nπ)		Γ(Δπ)		Γ(Nρ)		Γ(Nε)		Γ(other)	
		CERN	Saclay	CERN	Saclay	CERN	Saclay	CERN	Saclay	CERN	Saclay	CERN	Saclay	CERN	Saclay
Wave		S11				S11		SD11		SS11		SP11		(Nη) SS11	
K-Matrix Pole	Real	1502	1501	61.8	60.1	13.6	12.3	$.1^{+}$	0.0^{+}	1.9^{+}	1.8^{+}	1.0^{-}	1.5^{-}	$45.2^{\pm}$	$44.4^{\pm}$
T-Matrix Pole	Real	1499	1496	48.4	46.4	31.0	27.9	$.8^{+}$	$.4^{+}$	1.6^{+}	2.0^{+}	1.7^{-}	3.2^{-}	$13.3^{\pm}$	$12.8^{\pm}$
	Imag.	$\frac{-105i}{2}$	$\frac{-103i}{2}$	61.3i	45.0i	-19.6i	-26.4i	.3i	-.1i	6.3i	5.0i	2.5i	2.5i	71.8i	64.0i
	Mod.			|120.1|	|113.5|	|36.7|	|38.4|	|.9|	|.4|	|6.5|	|5.4|	|3.0|	|4.0|	|73.0|	|65.2|
K-Matrix Pole	Real	1684	1684	210.4	213.9	166.5	168.5	10.5^{-}	11.7^{-}	3.1^{-}	2.9^{-}	24.1^{-}	24.4^{-}	$6.2^{\pm}$	$6.5^{\pm}$
T-Matrix Pole	Real	1651	1648	44.7	36.4	38.9	32.4	2.1^{-}	2.3^{-}	-2.0^{+}	-1.6^{+}	15.2^{-}	15.4^{-}	$-9.4^{\pm}$	$-12.1^{\pm}$
	Imag.	$\frac{-119i}{2}$	$\frac{-117i}{2}$	-75.4i	-84.2i	-50.1i	-52.3i	1.2i	1.0i	7.0i	4.7i	0.0i	-3.3i	-33.5i	-34.3i
	Mod.			|123.1|	|121.2|	|63.4|	|61.5|	|2.4|	|2.5|	|7.3|	|5.0|	|15.2|	|15.8|	|34.8|	|36.4|
K-Matrix Pole	Real	1973	1964	628.7	616.9	1.8	1.9	368.2^{+}	312.5^{+}	154.1^{+}	149.1^{+}	2.5^{-}	2.7^{-}	$102.1^{\pm}$	$150.7^{\pm}$
T-Matrix Pole	Real	1949	1937	13.2	8.0	8.9	.7	$.8^{+}$	2.1^{+}	-10.6^{+}	-13.3^{+}	-3.7^{+}	-2.0^{+}	$17.7^{\pm}$	$20.6^{\pm}$
	Imag.	$\frac{-131i}{2}$	$\frac{-139i}{2}$	-24.4i	-20.6i	-22.8i	-25.2i	10.5i	10.2i	-41.5i	-41.6i	31.6	34.4i	-2.2i	1.5i
	Mod.			|127.4|	|134.5|	|24.5|	|25.2|	|10.5|	|10.4|	|42.8|	|43.7|	|31.8|	|34.5|	|17.8|	|20.7|

Wave		P11				P11		PP11		PP11		PS11			
K-Matrix Pole	Real	1429	1431	597.7	583.9	90.5	90.7	74.6^{-}	73.0^{-}	301.2^{-}	288.9^{-}	131.4^{+}	131.3^{+}		
T-Matrix Pole	Real	1379	1381	65.3	70.0	45.0	49.8	11.6^{-}	11.4^{-}	12.0^{-}	12.1^{-}	-3.4^{+}	-3.3^{+}		
	Imag.	$\frac{-210i}{2}$	$\frac{-209i}{2}$	-115.7i	-115.7i	-127.6i	-126.8i	-7.5i	-7.4i	10.4i	9.5i	9.0i	9.2i		
	Mod.			|174.6|	|175.0|	|135.3|	|136.2|	|13.9|	|13.6|	|15.9|	|15.3|	|9.6|	|9.8|		
K-Matrix Pole	Real	1697	1693	283.9	235.7	9.2	12.5	53.3^{+}	39.8^{+}	43.7^{+}	30.2^{+}	177.7^{-}	153.2^{-}		
T-Matrix Pole	Real	1712	1708	-3.0	-1.0	-3.7	-2.7	3.1^{-}	3.7^{-}	2.3^{+}	2.6^{+}	-4.7^{-}	-4.6^{-}		
	Imag.	$\frac{-22i}{2}$	$\frac{-17i}{2}$	- .7i	2.3i	-4.6i	-1.9i	-4.9i	-2.7i	1.2i	1.1i	7.6i	5.8i		
	Mod.			|23.2|	|18.0|	|5.9|	|3.3|	|5.8|	|4.5|	|2.6|	|2.8|	|8.9|	|7.4|		

TABLE IV. (cont.)

Origin		Mass		Γ(total)		Γ($N\pi$)		Γ($\Delta\pi$)				Γ($N\rho$)		Γ($N\epsilon$)		Γ(other)	
		CERN	Saclay	CERN	Saclay	CERN	Saclay	CERN	Saclay	CERN	Saclay	CERN	Saclay	CERN	Saclay	CERN	Saclay
Wave		P13				P13						PP13					
K-Matrix Pole	Real	1766	1764	227.6	227.6	46.4	47.5					181.5^-	180.1^-				
T-Matrix Pole	Real	1716	1716	49.7	49.6	1.8	2.2					47.9^-	47.4^-				
	Imag.	$\frac{-126i}{2}$	$\frac{-124i}{2}$	-65.9i	-64.1i	-15.4i	-15.7i					-50.5i	-48.4i				
	Mod.			|85.1|	|83.6|	|15.5|	|15.8|					|69.6|	|67.7|				
Wave		D13				D13		DS13		DD13		DS13		DP13			
K-Matrix Pole	Real	1524	1530	258.5	264.2	78.9	81.0	104.6^+	90.7^+	62.3^+	76.7^+	$.7^-$	0.0^-	12.0^-	15.8^-		
T-Matrix Pole	Real	1511	1514	111.3	121.4	81.3	88.1	7.6^+	10.2^+	20.9^+	21.8^+	$-.2^+$	$-.2^+$	1.8^+	1.5^+		
	Imag.	$\frac{-137i}{2}$	$\frac{-146i}{2}$	-12.0i	-13.6i	4.7i	3.1i	12.7i	14.0i	-11.3i	-8.6i	-18.1i	-22.2i	0.0i	0.0i		
	Mod.			|139.9|	|152.7|	|81.4|	|88.1|	|14.8|	|17.4|	|23.8|	|23.4|	|18.1|	|22.2|	|1.8|	|1.5|		
K-Matrix Pole	Real	1743	1759	1551.8	1407.7	34.8	31.5	394.7^+	384.1^+	1052.9^-	933.7^-	41.6^-	23.4^-	27.8^+	35.0^+		
T-Matrix Pole	Real	1678	1710	87.7	167.1	-.5	-10.3	31.7^+	50.5^+	4.7^-	21.2^-	-7.1^-	-6.0^-	59.0^-	122.7^-		
	Imag.	$\frac{-567i}{2}$	$\frac{-607i}{2}$	-139.9i	-455.1i	-11.6i	- 9.3i	-9.4i	-58.2i	-8.3i	-49.8i	2.7i	1.5i	-113.4i	-339.4i		
	Mod.			|189.6|	|508.6|	|11.6|	|13.9|	|33.0|	|77.1|	|9.5|	|54.1|	|7.6|	|6.2	|127.9|	|357.3|		
Wave		D15				D15		DD15									
K-Matrix Pole	Real	1677	1676	156.3	142.3	64.2	59.4	92.1^-	82.9^-								
T-Matrix Pole	Real	1668	1663	193.3	152.6	76.4	60.0	117.0^-	92.7^-								
	Imag.	$\frac{-171i}{2}$	$\frac{-146i}{2}$	15.2i	-9.6i	-11.2i	-17.6i	26.5i	8.0i								
	Mod.			|197.1|	|155.5|	|77.2|	|62.5|	|119.9|	|93.0|								
Wave		F15				F15		FP15		FF15		FP15		FD15			
K-Matrix Pole	Real	1687	1685	153.6	147.3	80.3	81.0	2.7^+	7.8^+	1.3^+	1.4^+	43.6^+	25.5^+	25.7^-	31.6^-		
T-Matrix Pole	Real	1674	1668	132.3	121.7	79.6	72.7	10.9^+	15.1^+	-1.6^+	$.3^+$	17.4^+	10.1^+	25.9^-	23.6^-		
	Imag.	$\frac{-137i}{2}$	$\frac{-132i}{2}$	-35.4i	-42.9i	-9.1i	-19.5i	1.1i	.2i	-3.8i	-1.0i	-10.3i	-8.0i	-13.3i	-14.6i		
	Mod.			|144.6|	|132.0|	|80.1|	|75.3|	|11.0|	|15.1|	|4.1|	|1.0|	|20.2|	|12.8|	|29.1|	|27.8|		

TABLE IV. (cont.)

Origin		Mass		Γ(total)		Γ($N\pi$)		Γ($\Delta\pi$)		Γ($N\rho$)		Γ($N\epsilon$)	Γ(other)
		CERN	Saclay	CERN	Saclay	CERN	Saclay	CERN	Saclay	CERN	Saclay	Saclay	Saclay
Wave		S31				S31		SD31		SS31			
K-Matrix Pole	Real	1446	1439	2558.1	2490.3	6.0	8.1	61.0^{+}	49.2^{+}	2491.1^{+}	2433.0^{+}		
T-Matrix Pole	Real	1583	1583	21.6	21.9	-27.6	-26.6	73.6^{+}	71.3^{+}	-24.3^{-}	-22.8^{-}		
	Imag.	$\frac{-149i}{2}$	$\frac{-143i}{2}$	-67.0i	-66.i	-26.6i	-26.1i	-29.6i	-28.7i	-10.8i	-11.8i		
	Mod.			|144.3|	|139.8|	|38.3|	|37.3|	|79.3|	|76.9|	|26.6|	|25.6|		
K-Matrix Pole	Real	1685	1677	542.9	492.5	175.1	158.9	3.8^{+}	9.1^{+}	364.0^{-}	324.5^{-}		
T-Matrix Pole	Real	2025	2029	-157.3	-158.6	-18.4	-17.9	-102.4^{-}	-96.8^{-}	-36.5^{+}	-44.0^{+}		
	Imag.	$\frac{-163i}{2}$	$\frac{-164i}{2}$	-9.9i	-11.6i	- 9.7i	- 9.2i	16.3i	14.9i	-16.5i	-17.3i		
	Mod.			|164.6|	|165.3|	|20.8|	|20.1|	|103.7|	|97.9|	|40.1|	|47.3|		
Wave		P33				P33		PP33					
K-Matrix Pole	Real	1232	1232	112.8	113.9	112.8	113.9	0.0	0.0				
T-Matrix Pole	Real	1212	1212	88.1	88.4	88.1	88.4	0.0	0.0				
	Imag.	$\frac{-100i}{2}$	$\frac{-101i}{2}$	-38.7i	-39.5i	-38.7i	-39.5i	0.0i	0.0i				
	Mod.			|96.3|	|96.8|	|96.3|	|96.8|	|0.0|	|0.0|				
K-Matrix Pole	Real	1999	1998	3585.8	3593.9	245.3	244.5	3340.5^{-}	3349.4^{-}				
T-Matrix Pole	Real	1610	1609	8.6	5.9	19.8	17.4	-11.2^{-}	-11.5^{-}				
	Imag.	$\frac{-325i}{2}$	$\frac{-323i}{2}$	-233.1i	-231.8i	-76.0i	-74.9i	-157.1i	-157.0i				
	Mod.			|236.0|	|234.3|	|78.5|	|76.9|	|157.5|	|157.4|				
Wave		D33				D33		DS33		DD33		DS33	
K-Matrix Pole	Real	1567	1564	427.5	479.4	10.3	11.0	57.9^{-}	62.1^{-}	49.0^{+}	53.4^{+}	310.3^{+}	352.9^{+}
T-Matrix Pole	Real	1672	1681	85.8	89.6	33.6	34.5	93.4^{-}	98.9^{-}	-24.2^{-}	-22.8^{-}	-17.1^{+}	-20.9^{+}
	Imag.	$\frac{-241i}{2}$	$\frac{-245i}{2}$	133.5i	130.1i	5.6i	9.5i	54.7i	55.0i	-12.1i	-15.9i	85.4i	81.5i
	Mod.			|256.4|	|260.9|	|34.0|	|35.8|	|108.3|	113.1|	|27.0|	|27.8|	|87.0|	|84.2|
K-Matrix Pole	Real	1969	1969	235.1	267.8	24.2	23.8	161.1^{+}	188.7^{+}	7.5^{-}	15.8^{-}	42.3^{-}	39.5^{-}
T-Matrix Pole	Real	1926	1915	132.2	105.9	.4	.3	113.4^{+}	87.0^{+}	$-.9^{-}$	-1.3^{-}	19.2^{-}	20.0^{-}
	Imag.	$\frac{-186i}{2}$	$\frac{-190i}{2}$	-147.3i	-176.9i	-6.7i	-4.7i	-154.1i	-182.2i	1.4i	1.8i	12.1i	8.2i
	Mod.			|222.5|	|230.5|	|6.7|	|4.7|	|191.3|	|201.9|	|1.7|	|2.3|	|22.7|	|21.6|

TABLE IV. (cont.)

Origin		Mass CERN	Mass Saclay	Γ(total) CERN	Γ(total) Saclay	Γ(Nπ) CERN	Γ(Nπ) Saclay	Γ(Δπ) CERN	Γ(Δπ) Saclay	Γ(Nρ) CERN	Γ(Nρ) Saclay	Γ(Nε) CERN	Γ(Nε) Saclay	Γ(other) CERN	Γ(other) Saclay
Wave		F35				F35		FF35		FP35					
K-Matrix Pole		Real	1888	1894	459.5	471.0	58.8	59.1	0.0^{+}	0.1^{+}	400.7^{-}	411.8^{-}			
T-Matrix Pole	Real	1808	1813	103.5	108.6	20.9	21.7	36.5^{-}	38.0^{-}	46.0^{-}	48.9^{-}				
	Imag. $\frac{-187i}{2}$		$\frac{193i}{2}$	-91.1i	-93.0i	-22.8	-23.2i	11.3i	12.8i	-79.5i	-82.6i				
	Mod.			|161.1|	|167.9|	|30.9|	|31.7|	|38.2|	|40.1|	|91.9|	|96.0|			
Wave		F37				F37		FF37		FF37				(Δρ)FP37	
K-Matrix Pole		Real	1900	1900	550.7	550.8	102.3	102.0	203.2^{-}	201.6^{-}	64.4^{-}	65.1^{-}		$180.8^{\pm}$	$182.0^{\pm}$
T-Matrix Pole	Real	1924	1924	232.5	232.6	83.5	81.1	73.3^{-}	75.9^{-}	21.8^{-}	23.7^{-}			$53.9^{\pm}$	$51.9^{\pm}$
	Imag. $\frac{-258i}{2}$		$\frac{-258i}{2}$	-29.6i	-30.4i	-24.4i	-24.8i	-9.9i	-11.9i	29.7i	31.1i			-24.9i	-24.9i
	Mod.			|257.2|	|258.4|	|87.0|	|84.8|	|75.0|	|76.9|	|36.8|	|39.1|		|59.4|	|57.6|

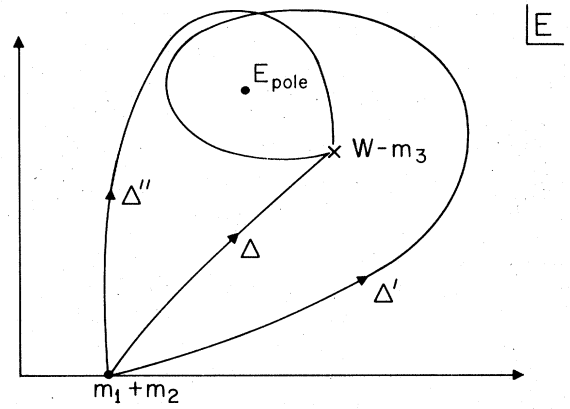

FIG. 4. Three different paths $\Delta, \Delta', \Delta''$ in the E plane. E is the diparticle mass that makes up the isobar. W is the complex $\sqrt{s}$ (three-body) where one searches for poles in the three-body T matrix.

In Fig. 4 we have drawn three different paths of integration and labeled them with the symbols $\Delta, \Delta', \Delta''$ as used for the integrals themselves, and in Fig. 5 we have deformed the three contours to show that they differ only by circles around the pole. Also in Fig. 5 we show a branch cut coming to the end point of integration which is due to the factor Q in the integral in the numerator of Eq. (5.1). Along Δ' we want Q to be continuous; but this means that Q is on a different sheet when the integration passes near the pole. So in order to define on which sheet $\Delta_{\alpha\alpha}$ is evaluated, we must specify both the sign of the imaginary part of Q at the lower limit of integration and also the path (Δ, Δ', or Δ'') of the integration. Summarizing Figs. 4 and 5, we find six sheets generated by three contours ($\Delta, \Delta', \Delta''$) and two possible signs for ImQ. However, we

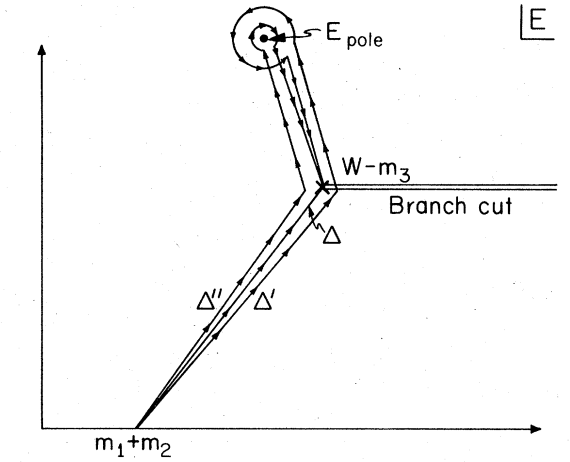

FIG. 5. The paths of Fig. 4 are deformed so that they differ only by integration around the pole.

only expect to find poles on the sheets with ImQ <0 for reasons of causality.

3. *Sheets in W plane*

Next we point out that all values of Δ, Δ', and Δ'' approach zero if the end point of integration (W-m_3) approaches E_{pole}. To see this, consider Eq. (5.1), which we write as $\Delta \equiv I/D$. Then D diverges as the end point approaches the pole (in $|T_\alpha|^2$), but the integrand of I contains a factor Q which always goes to zero at the end point and cancels the divergence of $|T_\alpha|^2$. Thus at the end point, Δ equals a finite number divided by infinity, which is zero. Hence, for Δ as a function of W, we have shown that its values $\Delta, \Delta', \Delta''$ all become equal at $W = E_{\text{pole}} + m_3$ so that $E_{\text{pole}} + m_3$ is the beginning of a branch cut (see Fig. 6). There is, of course, also a conjugate branch cut at $E = E^*_{\text{pole}} + m_3$, also drawn in Fig. 6.

Soon we shall discuss hunting in W, looking for a pole in T. Suppose we find a pole at W on the Δ sheet; in general there will be "shadow poles" at W' on the Δ' sheet and at W'' on Δ'', where W, W', W'' may be close. Hence we must understand the W-sheet structure of Fig. 8 to decide which of the poles is most influential at the real axis.

To understand Fig. 8, it is helpful to consider Fig. 7, a sketch of contours in the E plane. In Fig. 7, a dashed line starting at E_{pole} corresponds to the branch cut starting at $E_{\text{pole}} + m_3$ in Figs. 6 and 8. This line is no barrier to the contours $\Delta, \Delta', \Delta''$, but we cannot move the end point W-m_3 across this line without changing the names of the contour (changing sheets in the W plane).

Note that if W-m_3 is near the real axis the only short contour is Δ. Consequently the W sheet connecting to the physical region in Fig. 8 is

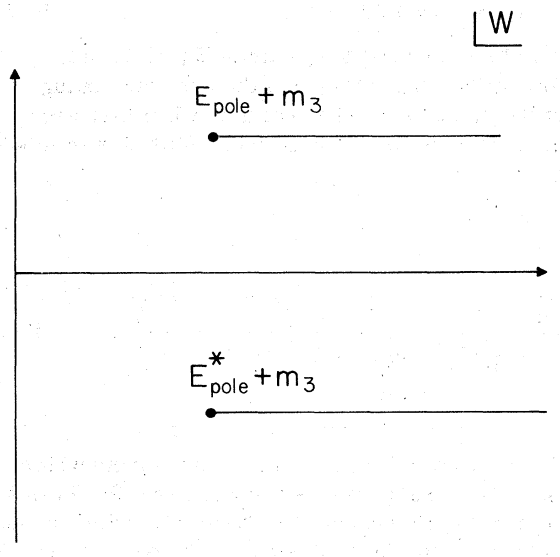

FIG. 6. The branch cuts in the $\sqrt{s}$ or W plane (total c.m. energy) generated by the pole in the final-state interaction of the isobar.

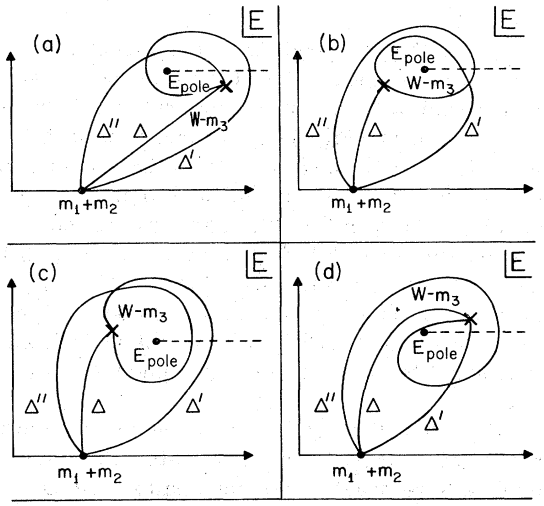

FIG. 7. Three different paths of integration in the E plane at four different values of W. The dashed line is the projection of the branch cut from the W plane which is not crossed by $W-m_3$ as it moves from (a) to (d).

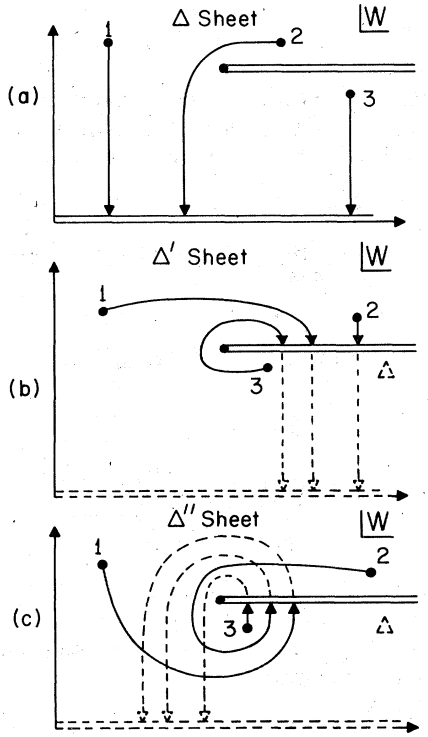

FIG. 8. Three points on the Δ, Δ', and Δ'' sheets and how one has to travel from them to the physical region in a continuous way.

labeled Δ.

To go further we need Figs. 7(a) through 7(d). In Fig. 7(a), the end point of the integral is below the dashed line. As we deform the contour from Fig. 7(a) to Fig. 7(d), the end point of the integral moves around the pole in the E plane. In Fig. 7(d) we are above the dashed line. If we consider point 3 in Fig. 8(a) and move it continuously up through the branch cut, we will change sheets. We see that the Δ contour in Fig. 7(a) deforms continuously into the Δ′ contour in Fig. 7(d). Thus point 3 of Fig. 8(a) would move from the Δ sheet to the Δ′ sheet, e.g., point 2 of Fig. 8(b).

In Figs. 8(a) through 8(c) we show three points on each of the Δ, Δ′, and Δ″ sheets. For each point we have drawn continuous paths leading to the physical region. In Figs. 8(b) and 8(c), when we pass onto the Δ sheet (the only sheet connected to the physical region) the lines are dashed. The length of the lines in Figs. 8(a) through 8(c) are a measure of how close a point is to the physical region. Therefore if we find a pole on Δ, Δ′, or Δ″, we can use Fig. 8 to tell us how close it is to the physical region.

In practice it is necessary to calculate only one contour integral. To show how this is done, let us define

$$\Delta \equiv I/D\,. \tag{5.7}$$

where I is the main integral and D is the denominator of Eq. (5.1). Call the denominator residue R_D; then, but using Cauchy's integral formula for contours Δ and Δ″, we obtain

$$D - D'' = 2\pi i R_D = 2\pi i \lim_{E \to E_{\text{pole}}} (E_{\text{pole}} - E)|T_{(E)}|^2 \frac{q(E)}{2}\,, \tag{5.8}$$

$$I - I'' = 2\pi i Q(W, E_{\text{pole}})\, B^2(W, E_{\text{pole}}) R_D\,. \tag{5.9}$$

We must be sure that we evaluate $Q(W, E_{\text{pole}})$ on the correct sheet. If we know Δ, R_D, and D, we can evaluate Δ″ by

$$\Delta'' = \frac{I''}{D''} = \frac{I - 2\pi i Q(W, E_{\text{pole}}) B^2(W, E_{\text{pole}}) R_D}{D(1 - 2\pi i R_D/D)}\,, \tag{5.10}$$

or

$$\Delta'' = \frac{\Delta - 2\pi i Q(W, E_{\text{pole}}) B^2(W, E_{\text{pole}}) R_D/D}{1 - 2\pi i R_D/D}\,. \tag{5.11}$$

In the case of Δ′ the spiral around E_{pole} is counterclockwise (see Figs. 4 and 5), so $2\pi i \to -2\pi i$, and that is the only change in the denominator D. In the main integral I, however, Q changes the sign because it is on the other sheet (see Fig. 5). Taking these into account, we get

$$\Delta' = \frac{\Delta - 2\pi i Q(W, E_{\text{pole}}) B^2(W, E_{\text{pole}}) R_D/D}{1 + 2\pi i R_D/D}\,. \tag{5.12}$$

Another property which may be demonstrated is that

$$\Delta(W) = -\Delta(W^*) \tag{5.13}$$

for all three contours Δ, Δ′, Δ″ and both signs of Q. Furthermore,

$$Q(W, E) = -Q^*(W^*, E^*) \tag{5.14}$$

for a given imaginary part of Q. This follows from

$$Q^2(W, E) = Q^2(W^*, E^*)\,. \tag{5.15}$$

All other terms that appear in Eq. (5.1) are Hermitian. Thus they are the complex conjugate of the value above the real axis when they are integrated below the real axis. With this in mind, we have

$$\frac{\frac{1}{4W}\int_{m_1+m_2}^{W-m_3} |T(E)|^2 Q(W, E) \frac{q(E)}{2} B^2(W, E) dE}{\int_{m_1+m_2}^{W-m_3} |T(E)|^2 \frac{q(E)}{2} dE} = -\left(\frac{\frac{-1}{4W^*}\int_{m_1+m_2}^{W^*-m_3} |T(E)|^2 Q(W^*, E) \frac{q(E)}{2} B^2(W^*, E) dE}{\int_{m_1+m_2}^{W^*-m_3} |T(E)|^2 \frac{q(E)}{2} dE} \right)^*\,. \tag{5.16}$$

Therefore Eq. (5.14) is true by the way we constructed our integrals.

C. Poles

To illustrate sheets and poles in our model, we will take the $F15$ amplitude as an example. The $F15$ resonance lies near the ρN threshold which is $\sqrt{s} = (1700 - i54)$ MeV as shown in Fig. 9. When we did the T-pole search, we found $F15$ poles on each (Δ, Δ′, Δ″, for $\text{Im}Q < 0$) sheet. The pole on the sheet generated by the Δ contour is closest to the physical region. Figure 9 shows the sheet structure and continuous paths going to the different

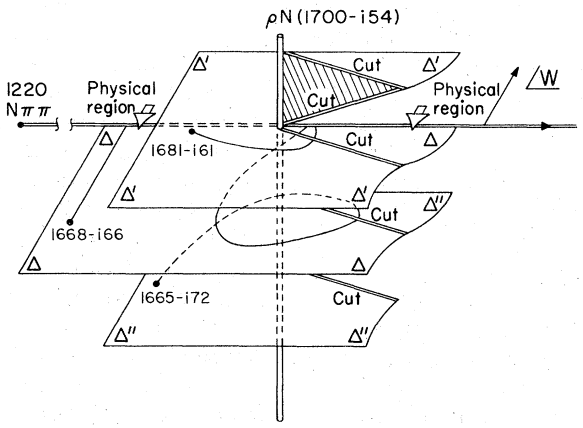

FIG. 9. The poles of the $F15$ T matrix which lie near ρN threshold. Each sheet is generated by the ρN cut.

poles on the different sheets. The poles and corresponding sheets are $1668-i\,66$ (Δ), $1681-i\,61$ (Δ'), and $1665-i\,72$ (Δ''). The path from the physical region to the pole on the Δ'' sheet is drawn in such a way as to reveal where it crosses the branch cut. All poles reported in this paper are those closest to the physical region.

Table IV gives a summary of the K-matrix and the T-matrix poles for solution B using both the CERN and the Saclay EPSA. Further discussion of these parameters is described in Sec. VI. The coupling signs and other sign conventions are explained in Sec. VII.

VI. BREIT-WIGNER REFIT

This section discusses how we refitted the smooth T matrix obtained from the K-matrix fit with an amplitude which is a sum of a unitary background and a Breit-Wigner form, rotated in such a way as to ensure unitarity for the total amplitude. Once the refits are performed, the resonance parameters obtained from the K matrix, the T-matrix poles, and the Breit-Wigner refit can be compared. The motivation for these comparisons was to find out how sensitive the resonance parameters are to the prescription from which they are obtained.

A. U(UB + BW) amplitude

In the past, resonances were parametrized by the Breit-Wigner form. The Breit-Wigner form by itself is unitary. Since there is always a background present due to other singularities, the T matrix is in general a sum of a Breit-Wigner form plus background. Because this is not evidently a unitary prescription, we have turned to the K matrix. Now that we have made the K-matrix fits and obtained a smooth description of the data, we would like to know what the Breit-Wigner parameters are for comparison with theoretical predictions. For this purpose we used a unitary amplitude consisting of a Breit-Wigner form and a unitary background with no local poles denoted by U(UB+BW). Since we believe that the background should not be affected locally by the presence of the resonance, we assumed that it is unitary with no local poles. In order to construct U(UB+BW), the Breit-Wigner form was permitted to rotate by energy-dependent phases (we believe that the Breit-Wigner form, and not the background, must accommodate itself to unitarity). These phases are calculated by the Davies-Baranger[17] constraint equation; also, see Goebel and McVoy.[17] Once we have made a K-matrix fit, we then refit using U(UB+BW) to the smooth T matrix in the region of the pole, in order to extract the Breit-Wigner parameters.

Let us assume we have a unitary background S matrix B_{ij}, and a Breit-Wigner form given by

$$R_{ij} = \frac{\frac{1}{2}\Gamma_i\Gamma_j}{(ER-E) - \frac{1}{2}i\sum_k \gamma_k^2 Q_k}\,,$$

$$\text{where } \Gamma_j = Q_j^{1/2}\gamma_j e^{i\theta_j}\,, \quad (6.1)$$

where all terms are real except Γ_j.

The Davies-Baranger constraint equation is

$$\sum_j B_{ij}\Gamma_j^* = \Gamma_i\,. \quad (6.2)$$

Let us relate B_{ij} to the background T matrix T:

$$B_{ij} = \delta_{ij} + 2iQ_i^{1/2}Q_j^{1/2}T_{ij}\,. \quad (6.3)$$

Now if we substitute Eqs. (6.1) and (6.3) into Eq. (6.2), we obtain

$$\sum_j (\delta_{ij} + 2iQ_i^{1/2}Q_j^{1/2}T_{ij})\gamma_j Q_j^{1/2}e^{i\theta_i}\,, \quad (6.4)$$

which can be shown to be equal to

$$\gamma_i \sin\theta_i = \sum_j Q_j\gamma_j T_{ij}e^{-i\theta_j}\,. \quad (6.5)$$

The right-hand side of Eq. (6.5) seems at first to be a complex number, but the left-hand side is real. So we can set the imaginary part of the right-hand side equal to zero, i.e.,

$$\sum_j Q_j\gamma_j \operatorname{Im}(T_{ij})\cos\theta_j - \sum_j Q_j\gamma_j \operatorname{Re}(T_{ij})\sin\theta_j = 0\,. \quad (6.6)$$

At this point we assume that Q_j is real. This means we must restrict ourselves to energies such that the jth channel is open ($Q_j^2 > 0$). We now define the vectors

$$(\sin) = \begin{bmatrix} \sin\theta_1 \\ \sin\theta_2 \\ \vdots \end{bmatrix}$$

and (6.7)

$$(\cos) = \begin{bmatrix} \cos\theta_1 \\ \cos\theta_2 \\ \vdots \end{bmatrix}$$

and the matrices

$$(\mathrm{Re}) = \begin{bmatrix} Q_1\gamma_1 \mathrm{Re}(T_{11}) & Q_2\gamma_2 \mathrm{Re}(T_{12}) \cdots \\ Q_1\gamma_1 \mathrm{Re}(T_{12}) & Q_2\gamma_2 \mathrm{Re}(T_{22}) \cdots \\ \vdots & \vdots \ddots \end{bmatrix}$$

and

$$(\mathrm{Im}) = \begin{bmatrix} Q_1\gamma_1 \mathrm{Im}(T_{11}) & Q_2\gamma_2 \mathrm{Im}(T_{12}) \cdots \\ Q_1\gamma_1 \mathrm{Im}(T_{12}) & Q_2\gamma_2 \mathrm{Im}(T_{22}) \cdots \\ \vdots & \vdots \ddots \end{bmatrix} \quad (6.8)$$

Equation (6.6) then becomes

$$(\mathrm{Im})(\cos) - (\mathrm{Re})(\sin) = 0 \quad (6.9)$$

or

$$(\cos) = (\mathrm{Im})^{-1}(\mathrm{Re})(\sin). \quad (6.10)$$

In addition we have the added constraints between the sine and the cosine,

$$\cos^2\theta_i + \sin^2\theta_i = 1. \quad (6.11)$$

Unfortunately we were, in general, unable to solve these transcendental equations. Therefore we imposed upon Eqs. (6.10) and (6.11) a χ^2 constraint and parametrized θ_i as a polynomial in W.

We were also interested in looking for the pole in $T = U(\mathrm{UB}+\mathrm{BW})$ (which is just the pole in the Breit-Wigner term) in the complex W plane. Since the $U(\mathrm{UB}+\mathrm{BW})$ amplitude must be Hermitian, θ_i must have the same real axis cut structure as Q_i [or Δ_{ii}; see Eq. (5.13)]. Therefore a natural parametrization for θ_i would be

$$\theta_i(W) = Q_i(W)\sum_{n=0}^{m} a_n W^n. \quad (6.12)$$

B. $D15$, $F35$, and $F15$ refit (solution A)

Having established this system, a series of K-matrix fits and Breit-Wigner refits were performed on three well-established resonances which were coupled to two, three, or four channels. We used the $D15$, $F35$, and $F15$ resonances. The results of these fits and refits are given in Table V. In line one of Table V we have identified the pole term of the K matrix with Breit-Wigner–type resonance parameters: The mass is the location of the pole, E_r, the ith partial width is just (kinematics) $\times\gamma_i^2$, and the total width is the sum of the partial widths. From this K-matrix fit we looked at the T-matrix pole where the real part of the pole position is identified with a mass; twice the imaginary part is identified with the total width (pole position is recorded in the mass column of Table V). From the residue of the T-matrix pole we defined the partial width as discussed in the first part of Sec. V. We record the real part, the imaginary part, and the modulus of partial width in Table V. For the total width we record the sum of the real parts, the imaginary parts, and the moduli of each partial width. For this T matrix we do a $U(\mathrm{UB}+\mathrm{BW})$ refit from one-half width before the pole (in the T matrix) to one-half width after the pole. We then obtain Breit-Wigner parameters (mass, partial widths, and total width) which are recorded in Table V. For the Breit-Wigner term of the refit, we look at the pole in the complex W plane thus recording the pole position and residue-related partial widths as we did for the T matrix. Next we refit the T matrix again, but this time relaxing the Davies-Baranger constraint, thus performing a UB+BW refit where the θ_i's are now constrant with energy. From this Breit-Wigner refit we record the fitted parameters and the pole parameters. Finally we went back to the K-matrix fit and took out all the inelastic amplitudes, thus performing a fit only to the elastic data.[13,14] In order to absorb the inelastic part, we added an unconstrained $\Delta\pi$ channel. We then went through the same series of refits and pole searches except for leaving out the $U(\mathrm{UB}+\mathrm{BW})$, since we only wanted to fit the elastic channel.

Figure 10 shows the Argand diagrams obtained from the $U(\mathrm{UB}+\mathrm{BW})$ refit to the $F35$ wave. The solid line is the total amplitude from 1740–1900 MeV (one-half width below T-matrix pole to one-half width above). The dashed line is the background for the same energy range. Arrows show the direction of increasing energy. Let us define $\Delta\theta_i$ as the change of rotation angle θ_i of the Breit-Wigner fit over the range of refit. Then

$$\Delta\theta_i = \theta_i(W = |W_{\mathrm{pole}}|) - \theta_i(W = |W_{\mathrm{pole}}| - 2\,\mathrm{Im}(W_{\mathrm{pole}})), \quad (6.13)$$

where W_{pole} is the pole position in the T matrix.

TABLE V. Comparison of parameters of K-matrix, T-matrix, and Breit-Wigner refit, all in MeV.

Origin			Mass		Γ(total)		Γ($N\pi$)		Γ($\Delta\pi$)		Γ($N\rho$)	Γ($N\epsilon$)
			CERN	Saclay	CERN	Saclay	CERN	Saclay	CERN	Saclay	CERN Saclay	CERN Saclay
2 channel, small background, D15(EPSA) + $N\pi\pi$												
Wave			D15				D15		DD15			
	K-matrix pole[a]	Real	1684	1683	161	153	66	64	95^-	89^-		
K-Matrix Fit												
	T-Matrix Pole[b]	Real	1666	1662	159	127	68	56	91^-	71^-		
		Imag.	$-\frac{159i}{2}$	$\frac{140i}{2}$	-24i	-39i	-14i	-18i	-10i	-21i		
		Mod.			|161|	|133|	|69|	|59|	|92|	|74|		
U(UB+BW) Fit	Unitarized BW parameters	Real	1692	1684	176	153	71	64	105^-	89^-		
	Unitarized BW pole[b]	Real	1666	1663	156	130	68	56	88^-	74^-		
		Imag.	$-\frac{158i}{2}$	$-\frac{140i}{2}$	-24i	-36i	-12i	-18i	-11i	-18i		
		Mod.			|158|	|135|	|69|	|59|	|89|	|76|		
UB+BW Fit	BW parameters	Real	1683	1684	167	153	68	64	99^-	89^-		
	BW Pole[b]	Real	1659	1662	134	127	57	55	77^-	71^-		
		Imag.	$-\frac{150i}{2}$	$-\frac{140i}{2}$	-45i	-40i	-22i	-18i	-23i	-22i		
		Mod.			|141|	|133|	|61|	|58|	|80|	|75|		
Wave			D15				D15		DD15		D15 (EPSA) only	
	K-Matrix Pole	Real	1682	1682	156	154	64	64	92	90		
K-Matrix Fit												
	T-Matrix Pole[b]	Real	1660	1660	125	122	54	53	71	69		
		Imag.	$-\frac{140i}{2}$	$-\frac{138i}{2}$	-43i	-44i	-20i	-20i	-23i	-24i		
		Mod.			|133|	|129|	|58|	|56|	|75|	|73|		
	BW parameters	Real	1682	1684	153	150	63	62	90	88		
UB+BW Fit	BW Pole[b]	Real	1661	1663			55	56				
		Imag.	$-\frac{140i}{2}$	$-\frac{143i}{2}$			-18i	-15i				
		Mod.					|58|	|58|				

TABLE V. (cont.)

Origin			Mass CERN	Mass Saclay	Γ(total) CERN	Γ(total) Saclay	Γ($N\pi$) CERN	Γ($N\pi$) Saclay	Γ($\Delta\pi$) CERN	Γ($\Delta\pi$) Saclay	Γ($N\rho$) CERN	Γ($N\rho$) Saclay	Γ($N\epsilon$) CERN	Γ($N\epsilon$) Saclay
4 channel, medium background, F15 (EPSA) + N$\pi\pi$														
Wave			F15				F15		FP15		FP15		FD15	
K-Matrix Fit	K-Matrix Pole[a]	Real	1684	1682	156	152	83	81	5^+	7^+	53^+	50^+	15^+	14^+
	T-Matrix Pole[b]	Real	1672	1669	152	138	99	89	5^+	7^+	33^+	30^+	15^+	12^+
		Imag.	$\frac{-155i}{2}$	$\frac{-145i}{2}$	-49i	-51i	-17i	-20i	11i	9i	-27i	-25i	-16i	-15i
		Mod.			|176|	|161|	|101|	|91|	|12|	|12|	|42|	|39|	|21|	|19|
	Unitarized BW parameters	Real	1681	1678	149	142	86	81	16^+	16^+	31^+	30^+	16^+	15^+
U(UB+BW) Fit	Unitarized BW Pole[b]	Real	1672	1669	148	137	92	84	7^+	8^+	37^+	35^+	12^+	10^+
		Imag.	$\frac{-148i}{2}$	$\frac{-140i}{2}$	-33i	-35i	-11i	-12i	8i	7i	-14i	-15i	-14i	-15i
		Mod.			|162|	|151|	|92|	|85|	|11|	|11|	|40|	|38|	|19|	|17|
	BW parameters	Real	1679	1679	148	141	84	80	12^+	12^+	36^+	34^+	16^+	15^+
UB+BW Fit	BW Pole[b]	Real	1672	1672	152	144	93	87	10^+	10^+	37^+	35^+	13^+	12^+
		Imag.	$\frac{-147i}{2}$	$\frac{-140i}{2}$	-30i	-25i	-10i	-7i	-9i	-9i	-18i	-16i	-11i	-11i
		Mod.			|165|	|154|	|93|	|87|	|14|	|14|	|41|	|38|	|17|	|16|
Wave			F15				F15		FP15		F15 (EPSA) only			
K-Matrix Fit	K-Matrix Pole	Real	1693	1692	183	179	107	104	77	75				
	T-Matrix Pole[b]	Real	1659	1658			70	64						
		Imag.	$\frac{-128i}{2}$	$\frac{-121i}{2}$			-24i	-26i						
		Mod.					|74|	|69|						
	BW parameters	Real	1678	1677	135	128	82	77	53	50				
UB+BW Fit	BW Pole[b]	Real	1664	1665			75	71						
		Imag.	$\frac{-129i}{2}$	$\frac{-122i}{2}$			-15i	-13i						
		Mod.					|77|	|73|						

TABLE V. (cont.)

Origin			Mass CERN	Mass Saclay	Γ(total) CERN	Γ(total) Saclay	Γ(Nπ) CERN	Γ(Nπ) Saclay	Γ(Δπ) CERN	Γ(Δπ) Saclay	Γ(Nρ) CERN	Γ(Nρ) Saclay	Γ(Nε) CERN	Γ(Nε) Saclay
3 channel, large background, F35 (EPSA) + Nππ														
Wave			F35				F35		FF35		FP35			
	K-Matrix Pole[a]	Real	2169	2136	3401	2545	178	165	47^{+}	135^{+}	3177^{-}	2246^{-}		
K-Matrix Fit	T-Matrix Pole[b]	Real	1824	1832	35	35	36	36	19^{+}	16^{+}	-20^{-}	-17^{-}		
		Imag.	$\frac{-282i}{2}$	$\frac{-278i}{2}$	-148i	-152i	-26i	-25i	-17i	-19i	-105i	-108i		
		Mod.			|177|	|178|	|44|	|44|	|26|	|25|	|107|	|109|		
U(UB+BW) Fit	Unitarized BW parameters	Real	1907	1911	325	320	51	50	55^{+}	50^{+}	219^{-}	220^{-}		
	Unitarized BW Pole[b]	Real	1824	1833	53	50	43	46	16^{+}	15^{+}	-6^{-}	-11^{-}		
		Imag.	$\frac{-282i}{2}$	$\frac{-282i}{2}$	-143i	-146i	-27i	-25i	-12i	-14i	-99i	-106i		
		Mod.			|173|	|180|	|51|	|53|	|23|	|21|	|99|	|106|		
	BW parameters	Real	1957	1942	391	395	75	70	41^{+}	47^{+}	275^{-}	278^{-}		
UB+BW Fit	BW Pole[b]	Real	1783	1798	13	-10	37	39	18^{+}	15^{+}	-42^{-}	-64^{-}		
		Imag.	$\frac{-386i}{2}$	$\frac{-363i}{2}$	-304i	-209i	-62i	-52i	-36i	-36i	-206i	-202i		
		Mod.			|323|	|316|	|72|	|65|	|41|	|39|	|210|	|212|		
Wave			F35				F35		FF35		F35 (EPSA) only			
	K-Matrix Pole	Real	2042	2062	1746	1808	154	156	1592	1652				
K-Matrix Fit	T-Matrix Pole[b]	Real	1810	1822			33	35						
		Imag.	$\frac{-275i}{2}$	$\frac{-283i}{2}$			-25i	-26i						
		Mod.					|42|	|43|						
	BW parameters	Real	1891	1901	300	291	36	35	264	256				
UB+BW Fit	BW Pole[b]	Real	1815	1833			20	22						
		Imag.	$\frac{-222i}{2}$	$\frac{-219i}{2}$			-13i	-11i						
		Mod.					|24|	|24|						

a. K-matrix parameters from Solution A which are reported in Longacre's thesis.
b. T-matrix pole has complex position and partial width (Γ_i). Modulus of Γ(total) is the sum of the moduli Γ_i.

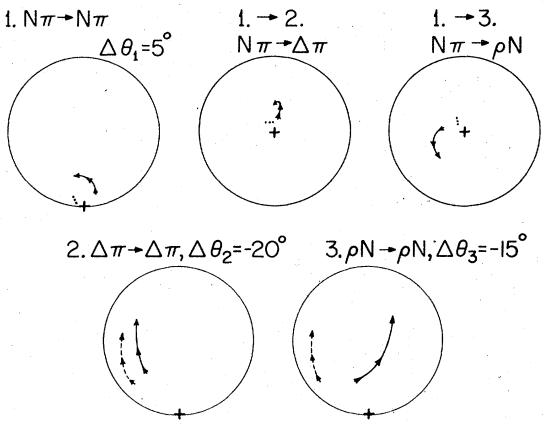

FIG. 10. Argand diagrams from the U(UB+BW) refit to the $F35$ wave. Solid line is the U(UB+BW) amplitude, while dashed line is the unitary background UB. Energy range is from 1740 to 1900 MeV, where arrows point direction of increasing energy. $\Delta\theta_i$ is the change of rotation angle of the Breit-Wigner fit in this energy range [Eq. (65)].

$\Delta\theta_i$ is plotted next to the elastic Argand diagrams of Fig. 10.

The results for the three resonances for both CERN and Saclay EPSA input are listed in Table V. Note that the pole position and residues for the T matrix from both the K matrix and U(UB+BW) are very close to each other. This is similar to the observation of Ball and Shaw[18] for the $P33$ resonance of the $N\pi$ system. A word of warning is necessary. These U(UB+BW) refits exactly reproduced the K-matrix solution with a smooth parametrization in the region of the pole. This would not be the case if we refitted our data. Appendix D shows how small fluctuations cause rapid shift in the pole position. The K-matrix parameters for the $F35$ have very little to do with the actual resonance parameters. This is because the background term in the K matrix is very large, and we have shown in Appendix D of Ref. 16 that the background term couples directly into the pole position of the T matrix. Also, one can easily show that the K-matrix pole is not stable under change of dimensionality (see Appendix **E**). For these reasons the resonance parameters obtained from T-matrix poles and U(UB+BW) refits are the best candidates for checking theoretical predictions. Since they disagree by factors of 2 with each other, we would not expect theory to do any better.

VII. SIGN OF COUPLINGS

One possible prescription for extracting the signs of resonance couplings (for the different channels) from the total T matrix near a resonance energy is discussed in this section. These signs are important for comparison with theory. The following is a summary of our procedure and conventions.

When the analysis was begun the set of partial waves had an arbitrary overall phase at each energy. This arbitrariness was resolved by the K-matrix fit. The resulting complete set of diagrams, however, was still determined only to within an overall arbitrary sign.[19] We chose $PP11$ ($\Delta\pi$) to be "up," thus fixing the orientation of the other diagrams relative to this amplitude.

A (+) or (−) sign appears in the *upper left-hand* corner of the inelastic diagrams in Fig. 3. Its origin is as follows. Inside our programs a certain arbitrary convention was used[1] to construct the three-particle final states in the angular momentum representations. We then had to switch to the "baryon-first" convention. This switch, in general, affects the Clebsch-Gordan coefficients and gives rise to the upper-left sign indicated in the diagrams. An Argand amplitude shown in our "internal" diagram must therefore be multiplied by its corresponding upper-left sign to convert it to the baryon-first convention.

We now come to the *coupling* signs. For the K matrix, the sign in the upper right-hand corner of the box in Table IV (where the partial width is shown) comes from the real K-matrix coupling of Eq. (2.21) and has already been changed to the baryon-first convention. These parameters and the signs are so meaningless that they were not even tabulated in Ref. 6.

The T-matrix coupling signs, indicated in the upper right-hand corner of the box in Table IV, come from the off-diagonal terms of the residue matrix and again have been changed to the baryon-first convention. These signs correspond to the method III of Ref. 6.

One can also read the sign directly off the Argand diagrams of Fig. 3 and multiply this coupling sign by the sign to change to the baryon-first convention given in the upper left-hand corner.

However, the resonance is not always necessarily pointing up or down. In these cases one could do a unitary Breit-Wigner refit to determine the sign of the resonance coupling. But this is really not necessary because if we can see the resonance shape we should be able to guess the resonance rotation angles θ_i. We see from Eq. (6.1) that the angles should be measurable by comparing the elastic and the inelastic channels. In the elastic channel (A_{11}) the resonance is rotated by $2\theta_1$, and in the inelastic channels (A_{1i}) the resonance is rotated by $\theta_1+\theta_i$. It is clear that θ_i has a range from $-90°$ to $90°$. Thus by determining these angles we will fix the sign of the

TABLE VI. List of partial width times sign of coupling (in MeV) and the angle of rotation of the Breit-Wigner form from eyeball fit.

		$N\pi$		$\Delta\pi$				ρN		ϵN		Other	
Mass (MeV)	Γ_{total}	$\Gamma_{N\pi}$	$\phi_{N\pi}$	$\Gamma_{\Delta\pi}$	$\phi_{\Delta\rho}$	$\Gamma_{\Delta'\pi}$	$\phi_{\Delta'\pi}$	$\Gamma_{\rho N}$	$\phi_{\rho N}$	$\Gamma_{\epsilon N}$	$\phi_{\epsilon N}$	Γ_{Other}	ϕ_{Other}
Wave		$S11$		$SD11$				$SS11$		$SP11$			
1510	100	20	0°	−2	−80°			+4	0°	−4	0°	±70	55°
1660	130	58	−22°	−6	0°			+8	65°	−18	0°	±40	−55°
Wave		$P11$		$PP11$				$PP11$		$PS11$			
1390	200	110	−30°	−50	−40°			−20	10°	+20	70°		
1710	75	15	−70°	−15	0°			+15	40°	+30	70°		
Wave		$P13$						$PP13$					
1720	150	30	−45°					−120	−25°				
Wave		$D13$		$DS13$		$DD13$		$DS13$		$DP13$			
1520	150	90	0°	+15	0°	+23	−45°	+15	−40°	+7	0°		
1710	300	30	−45°	+75	−45°	−60	−45°	−15	−45°	−120	−45°		
Wave		$D15$		$DD15$									
1660	150	67	−10°	−83	−10°								
Wave		$F15$		$FP15$		$FF15$		$FP15$		$FD15$			
1670	130	78	−5°	+13	0°	−1	0°	+19	0°	−19	0°		
Wave		$S31$		$SD31$				$SS31$					
1600	150	60	−60°	60	−10°			−30	−60°				
Wave		$P33$		$PP33$									
1640	300	30	−45°	−270	−45°								
Wave		$D33$		$DS33$		$DD33$		$DS33$					
1680	240	48	−15°	−72	15°	−12	−75°	+108	55°				
Wave		$F35$		$FF35$				$FP35$					
1830	220	40	−15°	−48	0°			−132	−35°				
Wave		$F37$		$FF37$				$FF37$				$\Delta\rho FP37$	
1925	240	96	−5°	−60	60°			−36	−70°			±48	0°

couplings. We have seen that once we made the unitary Breit-Wigner refit, the total T matrix produced by this method was very close to the T matrix produced by the K matrix.

Thus we shall employ the simple interpretation of U(UB + BW) but determine the coupling sign directly from the T-matrix elements produced by the original K-matrix fits. In fact, for all the resonant waves which have been fitted, we have looked at the T matrix for all the elastic (including, e.g., $\Delta\pi \to \Delta\pi$) and inelastic channels and determined by eye what the nominal values of the θ's are. This procedure is essentially the one given in methods I and II of Ref. 6. Table VI gives a list of the signs of the couplings and the angles from this eyeball fit. If the nominal value of θ is within ±30°, we think we are safe in determining the sign. But if the value of θ is greater than ±60°, the sign is questionable.

VIII. PREDICTED CHANNELS

In this section we discuss two K-matrix fits in which we introduced an extra channel in order to make up for the lack of cross section observed in the $N\pi\pi$ system. In the $S11$ wave we know[20] there must be a component of $N\eta$. In the $F37$ wave we assumed that the additional channel was $N\pi\pi\pi$.

The $P31$ has no evidence for resonance structure, and such a small cross section of it was observed in the isobar amplitudes that we did not do a K-matrix fit.

Around 1520 MeV a sizable amount of cross section goes into $N\eta$ (about 4 mb). In our K-matrix

fit to $S11$ we included the $N\eta$ channel[20] as a predicted channel (i.e., no input amplitude to constrain the χ^2). Our results are consistent around 1520 MeV with all the $N\eta$ cross section going into the $S11$ wave. The $S11$ amplitude for the $N\eta$ predicted from the K matrix is seen in Fig. 3.

In the 1900-MeV region we do not saturate the inelasticity of the $F37$ wave by 3 mb, so we introduced a predicted channel. In this energy region, 1900–2000 MeV, the $N\pi\pi\pi$ cross section grows from 4 to 6 mb,[21] so we made the predicted channel an $F37$ decaying by $\Delta\rho$ with angular momentum in a P wave. Thus our analysis forces a prediction of the amplitude for $F37$ decaying into the $N\pi\pi\pi$ via a $\Delta\rho$ decay in a P wave. The predicted Argand amplitude is shown in Fig. 3.

IX. CONCLUSIONS

We were able to apply the constraints of unitarity (using the K matrix) to isobar-model-generated amplitudes. We obtained a good representation of the Argand diagrams in almost all channels. These permitted us to remove the overall phase uncertainty of the inelastic amplitudes at each energy.

With a good representation of the T matrix we then could extract the pole parameters associated with resonant behavior in the Argand diagrams. The uniqueness of the pole parameters was demonstrated by doing Breit-Wigner refits to the fitted T-matrix amplitudes. Thus we found the same pole parameters in this alternative prescription. However, these refits showed, in general, that it was not possible to relate pole parameters unambiguously to the parameters of the Breit-Wigner fit. Furthermore, the success of the refits and the obvious interpretation of the amplitude U(UB+BW) (of Sec. VI) justified a simple determination of coupling sings from the fitted T-matrix (K-matrix-generated) amplitudes.

ACKNOWLEDGMENT

This work was supported by the U.S. Energy Research and Development Administration.

APPENDIX A: UNITARITY OF THE τ MATRIX

We wish to show that the τ matrix as defined in the text satisfies

$$\tau - \tau^+ = i\tau^+\Delta\tau . \tag{A1}$$

It was related to the K matrix by [see Eq. (2.13)]

$$\tau - k = \tfrac{1}{2} i\tau\Delta k . \tag{A2}$$

By definition the K matrix is real. The Δ matrix introduced in Eq. (2.15) is

$$\Delta_{\gamma\lambda} = \int f_\gamma \Phi_{\gamma\lambda} f_\lambda^* \, ds_\gamma \, ds_\lambda . \tag{A3}$$

Now it was shown in Ref. 8 that the recoupling coefficient Φ is Hermitian, i.e., $\Phi_{\gamma\lambda} = \Phi_{\gamma\lambda}^*$. From this it follows that Δ is also Hermitian, $\Delta = \Delta^+$. If we solve Eq. (A2) for the τ matrix, we obtain

$$\tau = k(1 - \tfrac{1}{2}\Delta k)^{-1} . \tag{A4}$$

Let us substitute Eq. (A4) into the left-hand side of Eq. (A1); we get

$$k(1 - \tfrac{1}{2} i\Delta k)^{-1} - (1 + \tfrac{1}{2} i k\Delta^+)^{-1} k \stackrel{?}{=} i\tau^+\Delta\tau . \tag{A5}$$

The next step is to introduce the unit matrices within [ ], in the appropriate places in the left-hand side of Eq. (A5):

$$[(1 + \tfrac{1}{2} ik\Delta^+)^{-1}(1 + \tfrac{1}{2} ik\Delta^+)]k(1 - \tfrac{1}{2} i\Delta k)^{-1} - (1 + \tfrac{1}{2} ik\Delta^+)^{-1} k[(1 - \tfrac{1}{2} i\Delta k)(1 - \tfrac{1}{2} i\Delta k)^{-1}] \stackrel{?}{=} i\tau^+\Delta\tau , \tag{A6}$$

or

$$(1 + \tfrac{1}{2} ik\Delta^+)^{-1}[(1 + \tfrac{1}{2} ik\Delta^+)k - k(1 - \tfrac{1}{2} i\Delta k)](1 - \tfrac{1}{2} i\Delta k)^{-1} \stackrel{?}{=} i\tau^+\Delta\tau , \tag{A7}$$

$$(1 + \tfrac{1}{2} ik\Delta^+)^{-1} \tfrac{1}{2}(ik\Delta^+ k) + \tfrac{1}{2}(ik\Delta k)(1 - \tfrac{1}{2} i\Delta k)^{-1} \stackrel{?}{=} i\tau^+\Delta\tau . \tag{A8}$$

Since Δ is a Hermitian matrix, we have

$$i(1 + \tfrac{1}{2} ik\Delta^+)^{-1} k\Delta k(1 - \tfrac{1}{2} i\Delta k)^{-1} = i\tau^+\Delta\tau . \tag{A9}$$

Finally, from Eq. (A4) we note that the matrices following Δ are just τ and the matrices preceding Δ are τ^+. Indeed Eq. (A1) is satisfied.

APPENDIX B: FACTORIZABLE RESIDUES

In this appendix we show that simple poles in the T matrix have factorizable residues.

The first step is to demonstrate that a factorizable matrix has only one nonzero eigenvalue. Consider a matrix B which has only one nonzero term B_{11}. Let U_{ij} be a unitary matrix. Consider the matrix B' such that

$$B' = U^+ B U . \tag{B1}$$

Using the condition that only the B_{11} term is nonzero, we obtain

$$B'_{ij} = U^*_{1i} B_{11} U_{1j} , \tag{B2}$$

or, rewritten another way,

$$B'_{ij} = (U^*_{1i}\sqrt{B_{11}})(\sqrt{B_{11}}\,U_{1j}) . \tag{B3}$$

It follows from Eq. (B3) that

$$B'_{ii}B'_{jj} = (B'_{ij})^2 . \tag{B4}$$

We shall use this result shortly.

It is clear that when we have a pole in the T matrix, the determinant of T^{-1} will be zero. We may diagonalize T^{-1} with a unitary matrix U.

$$T_D^{-1} = \begin{bmatrix} \lambda_1 & & \\ & \lambda_2 & 0 \\ & 0 & \lambda_3 \\ & & & \ddots \end{bmatrix} . \tag{B5}$$

The determinant $\mathrm{Det}(T_D^{-1})$ becomes

$$\mathrm{Det}(T^{-1}) = \lambda_1\lambda_2\lambda_3\cdots . \tag{B6}$$

If we have a simple zero at complex total center-of-mass energy $E = E_0$, then only one eigenvalue is equal to zero. By contrast a dipole (higher-order pole) would have two (many) zero eigenvalues. Therefore we may assume that one eigenvalue is given by

$$\lambda_1 = C(E - E_0) \tag{B7}$$

and the others are nonzero. Therefore the diagonal T^{-1} matrix can be written

$$T_D^{-1} = \begin{bmatrix} C(E-E_0) & & 0 \\ & \lambda_2 & \\ 0 & & \lambda_3 \\ & & & \ddots \end{bmatrix} , \tag{B8}$$

and the inverse is

$$T_D = \begin{bmatrix} \dfrac{1}{C(E-E_0)} & & 0 \\ & \dfrac{1}{\lambda_1} & \\ 0 & & \dfrac{1}{\lambda_2} \\ & & & \ddots \end{bmatrix} . \tag{B9}$$

The diagonal residue matrix is defined as

$$R_D = \lim_{E \to E_0} (E - E_0) T_D . \tag{B10}$$

From Eqs. (B9) and (B10), we get

$$\begin{bmatrix} \dfrac{1}{C} & & 0 \\ & \dfrac{(E-E_0)}{\lambda_2} & \\ 0 & & \dfrac{(E-E_0)}{\lambda_3} \end{bmatrix} = \begin{bmatrix} \dfrac{1}{C} & & 0 \\ & 0 & \\ 0 & & 0 \end{bmatrix} . \tag{B11}$$

Notice that the nondiagonal residue matrix is just

$$R = U^\dagger R_D U . \tag{B12}$$

From Eq. (C4) we know that it factorizes.

APPENDIX C: POLE AND RESIDUE FOR A SIMPLE BREIT-WIGNER FORM

In this appendix we discuss the shift of the pole parameters from the mass and width parameters of the Breit-Wigner fit. Also, we discuss possible definitions of the width and how it is related to the residue.

For simplicity we take a single-channel T matrix which is generated by a K matrix

$$T = \frac{K}{1 - i\Delta K} , \tag{C1}$$

where Δ is the kinematic factor. If we want a simple S-wave Breit-Wigner form, we need a simple pole in the K matrix without any barrier factors. Therefore we have

$$K = \frac{\Gamma/2}{E_R - E} , \tag{C2}$$

where E is the total center-of-mass energy and E_R is the K-matrix pole position. For Δ let us take a form that has a square root behavior and is equal to one at $E = E_R$:

$$\Delta = \left(\frac{E}{E_R}\right)^{1/2} . \tag{C3}$$

Substituting Eqs. (C2) and (C3) into (C1), we obtain

$$T = \frac{1}{(E_R - E)/\Gamma/2 - i(E/E_R)^{1/2}} . \tag{C4}$$

We know that we will have a pole in T when we have a zero in $D(E)$, the denominator of T. Let E_P be the value of E where $D(E)$ is equal to zero:

$$D(E_P) = 0 . \tag{C5}$$

Therefore

$$\frac{E_R - E_P}{\Gamma/2} = i\left(\frac{E_P}{E_R}\right)^{1/2} . \tag{C6}$$

Squaring both sides of Eq. (C6), we obtain

$$E_P^2 - 2\left(E_R - \frac{\Gamma^2}{8E_R}\right)E_P + E_R^2 = 0 , \tag{C7}$$

which can be solved by the binomial theorem

$$E_P = E_R\left(1 - \frac{\Gamma^2}{8E_R^2}\right) \pm \frac{i\Gamma}{2}\left(1 - \frac{\Gamma^2}{16E_R^2}\right)^{1/2} . \tag{C8}$$

If we make the narrow-width approximation ($E_R \gg \Gamma$), Eq. (C8) becomes

$$E_P = E_R\left(1 - \frac{\Gamma^2}{8E_R^2}\right) \pm \frac{i\Gamma}{2}\left(1 - \frac{\Gamma^2}{32E_R^2}\right) . \tag{C9}$$

Taking the root with the minus sign because we want the pole to be on the correct sheet, we see that E_P is given by

$$E_P = E_R\left(1 - \frac{\Gamma^2}{8E_R^2}\right) - \frac{i\Gamma}{2}\left(1 - \frac{\Gamma^2}{32E_R^2}\right). \tag{C10}$$

The real part of the pole position has been shifted by $-\Gamma^2/8E_R$ from the K-matrix pole position. Also, the width has been reduced in size by $\Gamma^3/32E_R^2$.

Next we expand $D(E)$ in a Taylor series about E_P.

$$D(E) = -\frac{\partial D}{\partial E}\bigg|_{E_P}(E_P - E) + \cdots , \tag{C11}$$

recalling that $D(E_P) = 0$. Differentiation of $D(E)$ and Eq. (C11) yields

$$D(E) \approx \left(\frac{2}{\Gamma} + \frac{i/2}{(E_P E_R)^{1/2}}\right)(E_P - E) . \tag{C12}$$

If we substitute into Eq. (C12) the expression E_P [Eq. (C10)] and assume that $E_R \gg \Gamma$ we obtain

$$D(E) = \left(\frac{2}{\Gamma} + \frac{i/2}{[E_R(E_R - i\Gamma/2)]^{1/2}}\right)(E_P - E) . \tag{C13}$$

Simplifying, we get

$$D(E) = \left(\frac{2}{\Gamma - i\Gamma^2/4E_R}\right)(E_P - E) . \tag{C14}$$

The residue at the pole is defined by

$$R = \lim_{E \to E_P} \frac{(E_P - E)}{D(E)} . \tag{C15}$$

Therefore we see that

$$R = \frac{\Gamma}{2} - \frac{i\Gamma^2}{8E_R} . \tag{C16}$$

The residue of the T matrix is related to the coupling of the resonance. We may define the coupling such that $\Gamma_{\text{total}} = 2\Delta \times$ (coupling). Now the question is: What momentum should we use in calculating the total width? For the coupling we used the residue of the pole, so one might think that the momentum at the pole should be used. On the other hand, the momentum on the real axis tells us how much of the coupling is physically seen.

We also know that the total width is associated with twice the imaginary part of the pole position, which is equal to

$$\Gamma_{\text{total}} = 2 \times \text{Im}(E_P) = \Gamma - \frac{\Gamma^3}{32E_R^2} . \tag{C17}$$

Using the Δ on the real axis evaluated at $\text{Re}(E_P)$ and the residue Eq. (C16), we obtain

$$\Gamma_{\text{total}} = \left(\frac{E_R - \Gamma^2/8E_R}{E_R}\right)^{1/2}\left(\frac{\Gamma}{2} - \frac{i\Gamma^2}{8E_R}\right) . \tag{C18}$$

Using $E_R \gg \Gamma$, we get

$$\Gamma_{\text{total}} = \Gamma - \frac{i\Gamma^2}{4E_R} - \frac{\Gamma^3}{16E_R^2} . \tag{C19}$$

Next we use Δ at the pole position

$$\Gamma_{\text{total}} = \left(\frac{E_R - \frac{\Gamma^2}{8E_R} - \frac{i\Gamma}{2} + \frac{i\Gamma^3}{64E_R^2}}{E_R}\right)^{1/2} \times \left(\frac{\Gamma}{2} - \frac{i\Gamma^2}{8E_R}\right) , \tag{C20}$$

where $E_R \gg \Gamma$. Thus

$$\Gamma_{\text{total}} = \Gamma - \frac{i\Gamma^2}{2E_R} - \frac{\Gamma^3}{8E_R^2} . \tag{C21}$$

It is clear that Δ on the real axis gives a total width with smaller imaginary part and magnitude closer to twice the imaginary part of E_P.

APPENDIX D: FLUCTUATIONS AND THE T-MATRIX POLES

In this appendix we show that the poles in the T matrix depend on how smoothly one parametrizes the T matrix. For example, let us take the well-known $N\pi$ resonance $P33$. The simplest form for the $P33$ resonance amplitude is

$$T = \frac{60}{1236 - E - i\,60} . \tag{D1}$$

For simplicity we have suppressed the kinematic dependence in the total width. This amplitude can be parametrized by an M matrix [see main text, Eq. (5.2)],

$$T=\frac{1}{m-i}\ . \tag{D2}$$

Again, for simplicity, q has been set equal to the value of 1. Therefore we have

$$M=\frac{1236-E}{60}\ . \tag{D3}$$

It is clear that we have a pole in the T matrix at $(1236-i\,60)$.

For the demonstration, we will add a small fluctuation to the M matrix. We can then write the M matrix as

$$M=\frac{1236-E}{60}\pm\epsilon\sin(n(E-1236))\ . \tag{D4}$$

The T matrix will now have a pole at $E=E_{\text{pole}}$, where

$$E_{\text{pole}}=1236\pm 60\epsilon\sin(n(E_{\text{pole}}-1236))-i\,60. \tag{D5}$$

If the fluctuations are small, we expect

$$E_{\text{pole}}\approx 1236-i\ 60\ . \tag{D6}$$

Substituting Eq. (D6) into the right-hand side of Eq. (D5), we find for the change in E_{pole} (ΔE_{pole})

$$\Delta E_{\text{pole}}\approx\pm\ 60\epsilon\sin(n(-i\,60)). \tag{D7}$$

Using the properties of the sine function, we have

$$\Delta E_{\text{pole}}\approx\pm 60\epsilon\left(\frac{e^{60n}-e^{-60n}}{2i}\right)$$

$$\approx\pm\, i\,30\epsilon e^{60n}\ . \tag{D8}$$

We see from Eq. (D8) that it is possible to have a large shift in the pole position due to small fluctuations in the M matrix if n is a large number. Why has this happened? An analytic function is determined by Laplace's equation. This means it has to have a boundary condition in order to be well determined. We have only defined the function on a short interval on the real axis. Because of this fact, we need an added assumption that the fluctuations in the M matrix must have a period equal to or greater than twice the particle energy spacing (smoothness assumption). Stated another way, fluctuations must arise only from particle structure. If one describes the experimental fluctuations in the real data too well, thus having a very small period, one will find poles which differ by a large amount in the complex plane.

APPENDIX E: THE K-MATRIX POLE AND ITS DEPENDENCY ON THE DIMENSIONALITY

In this appendix we show that the pole in the K matrix depends on the dimensionality of the K matrix. To demonstrate this simply, assume that we have an elastic scattering amplitude (T_{11}) which is generated by a two-channel factorizable K matrix

$$K_{ij}=\frac{\gamma_i\gamma_j}{E_R-E}\ . \tag{E1}$$

Therefore

$$T_{11}=\frac{q_1\gamma_1^{\,2}}{E_R-E-\,iq_1\gamma_1^{\,2}-i\,q_2\gamma_2^{\,2}}\ . \tag{E2}$$

Let us also assume that we are below the threshold of the second channel. This can be expressed by letting

$$q_2=i\,|q_2|\ . \tag{E3}$$

Substituting Eq. (E3) into Eq. (E2), we get

$$T_{11}=\frac{q_1\gamma_1^{\,2}}{E_R-E+\gamma_2^{\,2}|q_2|-i\,q_1\gamma_1^{\,2}}\ . \tag{E4}$$

If we now describe the amplitude by a single-channel K matrix,

$$T_{11}=\frac{1}{1/K-i\,q_1}\ , \tag{E5}$$

we will obtain an equally good fit to the data if

$$K=\frac{\gamma_1^{\,2}}{E_R+|q_2|\gamma_2^{\,2}-E}\ . \tag{E6}$$

It is clear that the two-channel K matrix has a pole at E_R while the single-channel K matrix has a pole at $E_R+|q_2|\gamma_2^{\,2}$.

The usual parametrization for a single-channel K matrix is

$$K=\frac{A}{E_p-E}+B\ . \tag{E7}$$

For our case we have

$$E_p=E_R+|q_2(E_p)|\gamma_2^{\,2}\ . \tag{E8}$$

We want

$$\frac{A}{E_p-E}+B=\frac{\gamma_1^{\,2}}{E_R+|q_2|\gamma_2^{\,2}-E}\ , \tag{E9}$$

where B does not have a pole at E_p. Solving Eq. (E9) for B, we get

$$B=\frac{\gamma_1^{\,2}(E_p-E)-A(E_R+|q_2|\gamma_2^{\,2}-E)}{(E_R+|q_2|\gamma_2^{\,2}-E)(E_p-E)}\ , \tag{E10}$$

where B has a pole at $E=E_p$. Using L'Hospital's

theorem, we can remove the pole from B by setting

$$A = \frac{\gamma_1^2}{1 - \frac{d|q_2(E_p)|}{dE}\gamma_2^2} . \tag{E11}$$

Thus we can describe the amplitude with a single-channel K matrix by letting

$$K = \frac{\gamma_1^2}{1 - \frac{d|q_2(E_p)|}{dE}\gamma_2^2} \frac{1}{E_p - E} + B . \tag{E12}$$

Therefore, both pole position and residue are dependent on the dimensionality we use.

APPENDIX F: DERIVATION OF EQUATION (2.5) OF THE MAIN TEXT

Starting with Eq. (60) of Ref. 1

$$d\sigma = \frac{\pi^2}{F} \bar{\sum_{\mu}} |f_\mu|^2 d\rho, \tag{F1}$$

and Eq. (43) of Ref. 1

$$f_\mu = \sum_n g_n^\mu(j) T_n(W, w_j) , \tag{F2}$$

we obtain by substitution and integration

$$\sigma = \int \frac{\pi^2}{Wp} \bar{\sum_{\mu}} \sum_j \sum_k \sum_n \sum_m g_n^\mu g_m^\mu T_n(W, w_i) \times T_m^*(W, w_k) d\rho . \tag{F3}$$

We note that although the indices n and m include the indices j and k [see Eq. (1) of Ref. 1], we will let them be separate for now.

If we take the sum over j and k and divide the double sum into a single sum over j and a double sum over j and k $(j \neq k)$, we obtain,

$$\sigma = \sum_j \int \frac{\pi^2}{Wp} \bar{\sum_{\mu}} \sum_{nm} g_n^\mu g_m^{\mu *} T_n(W, w_j) T_m^*(W, w_j) d\rho + \sum_{j \neq k} \int \frac{\pi^2}{Wp} \bar{\sum_{\mu}} \sum_{nm} g_n^\mu g_n^{\mu *} T_n(W, w_j) T_m^*(W, w_k) d\rho . \tag{F4}$$

The first term of the above equation has already been worked out in Appendix C of Ref. 1. The result is (for $\sigma_a = \frac{1}{2}$ and $\sigma_b = 0$)

$$\text{first term} = \frac{\pi}{p^2} \sum_n (J + \tfrac{1}{2}) \int |T_n^{JP}(W, w_j)|^2 \, dw_j^2 . \tag{F5}$$

We have suppressed the sum over j because the j index is now included in n. For the second term we have

$$\text{second term} = \frac{\pi^2}{Wp} \sum_{\substack{nm \\ j \neq k}} \int \bar{\sum_{\mu}} g_n^\mu g_m^{\mu *} T_n(W, w_j) \times T_m^*(W, w_k) d\rho. \tag{F6}$$

If we now pick for phase space $d\rho$ Eq. (31c) of Ref. 1, we have

$$\text{second term} = \frac{\pi^2}{p^2} \sum_{\substack{nm \\ j \neq k}} \int \bar{\sum_{\mu}} g_n^\mu g_m^{\mu *} T_n(W, w_j) T_m^*(W, w_k) \times \frac{1}{32W^2} dw_j^2 dw_k^2 \times d\cos\theta \, d\phi \, d\alpha . \tag{F7}$$

Since all the dependence of μ, $\cos\theta$, d, and α are contained in g_n^μ, we can sum and integrate over these variables. Thus we can write

$$\text{second term} = \frac{\pi^2}{Wp} \sum_{\substack{nm \\ j \neq k}} T_m^*(W, w_k) \left[\int \frac{\bar{\sum}_\mu g_n^\mu g_m^{\mu *} d(\cos\theta) d\phi \, d\alpha}{32W^2} \right] T_n(W, w_j) dw_j^2 \, dw_k^2 . \tag{F8}$$

The quantity in square brackets can be nonzero only for the states that have the same initial J^P quantum numbers. The reason is the same as that given in connection with the first term in Appendix C of Ref. 1. Thus we can redefine our normalization of T_n and g_n^μ and obtain Eq. (2.5) of the main text. It is also necessary to break up the single index n and m into an index that runs over the initial J^P state and the isobar channel:

$$\sigma = \frac{\pi}{4pW} \sum_{J^P} \left(J + \frac{1}{2} \right) \left[\sum_n \int |T_n^{JP}(W, w_n)|^2 \frac{Q_n q_n dw_n^2}{4W 4w_n} + \sum_n \sum_m \int \int T_m^{*JP}(W, w_m) \Phi_{mn}^{JP} T_n^{JP}(W, w_n) dw_m^2 dw_n^2 \right] . \tag{F9}$$

APPENDIX G: DERIVATION OF EQUATION (2.28) OF MAIN TEXT

In order to show why Eq. (2.28) is of the form it is, let us consider four channels $N\pi$, $\Delta_1\pi$, $\Delta_2\pi$, and $N\rho$, where $N\pi(n=1)$, $\Delta_1\pi(n=2)$, $\Delta_2\pi(n=3)$, and $N\rho(n=4)$ for a certain J^P state.

From Eq. (2.5) of the main text, we have

$$\sigma^{JP}=\frac{\pi}{4Q_1\sqrt{s}}\left(J+\frac{1}{2}\right)\Bigg(\int|T_{12}^{JP}|^2\,\frac{Q_2q_2ds_2}{4\sqrt{s}\;4\sqrt{s}}+\int|T_{13}^{JP}|^2\,\frac{Q_3q_3ds_3}{4\sqrt{s}\,4\sqrt{s_3}}+\int|T_{14}^{JP}|^2\,\frac{Q_4q_4ds_4}{4\sqrt{s}\;4\sqrt{s_4}}$$
$$+\int\int T_{12}^{JP}\phi_{23}^{JP}T_{23}^{JP}\,ds_2ds_3+\iint T_{12}^{JP}\phi_{24}^{JP}T_{14}^{JP}\,ds_2ds_4+\int\int T_{13}^{JP}\phi_{34}^{JP}T_{14}^{JP}\,ds_3ds_4$$
$$+\int\int T_{13}^{*JP}\phi_{12}^{*JP}\,ds_3ds_2+\int\int T_{14}^{*JP}\phi_{24}^{*JP}T_{12}^{JP}\,ds_4ds_2+\int\int T_{14}^{*JP}\phi_{34}^{*JP}T_{13}^{JP}\,ds_4ds_3\Bigg). \tag{G1}$$

For simplicity let us ignore the $\Delta_1\pi_1$ and $\Delta_2\pi_2$ interference term in the cross section because it is real and does not add anything more to the derivation than the combination of the $\Delta_1\pi_1$ and $\Delta_2\pi_2$ interference with the $N\rho$ system.

Using Eqs. (2.11), (2.14), (2.19), and (2.20) of the main text and substituting them into Eq. (G1), we obtain

$$\sigma^{JP}=\frac{\pi}{Q_1^{\,2}}\left(J+\tfrac{1}{2}\right)(|T_{12}|^2\Delta_{11}\Delta_{22}+|T_{13}|^2\Delta_{11}\Delta_{33}+|T_{14}|^2\Delta_{11}\Delta_{44}+T_{12}^*T_{14}\Delta_{11}\Delta_{24}$$
$$+T_{13}^*T_{14}\Delta_{11}\Delta_{34}+T_{14}^*T_{12}\Delta_{11}\Delta_{24}^*+T_{14}^*T_{13}\Delta_{11}\Delta_{34}^*)\,. \tag{G2}$$

Taking advantage of the fact that in the isospin space the two Δ contributions are equal and that we have built into our definition of the Δ matrix the Bose symmetry,[8] we know that $\Delta_{22}=\Delta_{33}$ and $\Delta_{24}=\Delta_{34}$. Therefore, we can write

$$\sigma^{JP}=\frac{\Delta_{11}\pi}{Q_1^{\,2}}\left(J+\tfrac{1}{2}\right)[(|T_{12}|^2+|T_{13}|^2)\Delta_{22}+(T_{12}^*+T_{13}^*)T_{14}\Delta_{24}+T_{14}^*(T_{12}+T_{13})\Delta_{24}^*+|T_{14}|^2\Delta_{44}]\,. \tag{G3}$$

This can be further reduced to

$$\sigma^{JP}=\frac{\Delta_{11}\pi}{Q_1^{\,2}}\left(J+\tfrac{1}{2}\right)\{(|T_{12}|^2+|T_{13}|^2)\Delta_{22}+2\,\mathrm{Re}[(T_{12}^*+T_{13}^*)T_{14}\Delta_{24}]+|T_{14}|^2\Delta_{44}\}\,. \tag{G4}$$

Again Bose symmetry implies that $T_{12}=T_{13}$. This means that T_{12} and T_{13} must add to give the interference term.

We can form a total Δ amplitude by adding T_{12} and T_{13}. However, we want to define a $T_{1\Delta}$ such that

$$\sigma_\Delta^{JP}=\frac{\Delta_{11}\pi}{Q_1^{\,2}}\left(J+\tfrac{1}{2}\right)|T_{1\Delta}|^2\Delta_{22}\,. \tag{G5}$$

It is clear that

$$|T_{1\Delta}|^2=|T_{12}|^2+|T_{13}|^2\,. \tag{G6}$$

This implies that

$$T_{1\Delta}=\frac{T_{12}}{\sqrt{2}}+\frac{T_{13}}{\sqrt{2}}\,, \tag{G7}$$

which is Eq. (2.28) of the main text.

Finally, the coupling of the K matrix for the two Δ states has been reduced by $1/\sqrt{2}$. This can be most simply shown, if we consider just a three-channel K matrix, where channel 1 is $N\pi$ and channels 2 and 3 are $\Delta_1\pi_1$ and $\Delta_2\pi_2$. If we only have one single pole in the K matrix and no Δ-Δ interference, the T matrix can be written as

$$T=\frac{\begin{bmatrix}\frac{\gamma_1\gamma_1}{2} & \frac{\gamma_1\gamma_2}{2} & \frac{\gamma_1\gamma_3}{2}\\ \frac{\gamma_1\gamma_2}{2} & \frac{\gamma_2\gamma_2}{2} & \frac{\gamma_2\gamma_3}{2}\\ \frac{\gamma_1\gamma_3}{2} & \frac{\gamma_2\gamma_3}{2} & \frac{\gamma_3\gamma_3}{2}\end{bmatrix}}{ER-W-\frac{1}{2}i\,(\Delta_{11}\gamma_1^{\,2}+\Delta_{22}\gamma_2^{\,2}+\Delta_{33}\gamma_3^{\,2})}\,. \tag{G8}$$

We want to replace this by a two-channel T matrix with just an $N\pi$ and a single $\Delta\pi$ channel

$$T = \frac{\begin{bmatrix} \frac{\gamma_1\gamma_1}{2} & \frac{\gamma_1\gamma_\Delta}{2} \\ \frac{\gamma_1\gamma_\Delta}{2} & \frac{\gamma_\Delta\gamma_\Delta}{2} \end{bmatrix}}{ER - W - \frac{1}{2}i(\Delta_{11}\gamma_1^2 + \Delta_{22}\gamma_\Delta^2)} . \quad \text{(G9)}$$

If we now consider Eq. (2.28) of the main text, we see that

$$\frac{\frac{\gamma_1\gamma_\Delta}{2}}{ER - W - \frac{1}{2}i(\Delta_{11}\gamma_1^2 + \Delta_{22}\gamma_\Delta^2)} = \frac{\frac{\gamma_1\gamma_2}{2\sqrt{2}} + \frac{\gamma_1\gamma_3}{2\sqrt{2}}}{ER - W - \frac{1}{2}i[\Delta_{11}\gamma_1^2 + \Delta_{22}(\gamma_2^2 + \gamma_3^2)]} . \quad \text{(G10)}$$

This equation implies that

$$\gamma_2 = \gamma_3 = \gamma_\Delta/\sqrt{2} .$$

---

*Present address: Department of Physics, Northeastern University, Boston, Mass. 02115.
†Present address: SLAC, Stanford University, Stanford, California 94305.
‡Present address: CEN, Saclay, B. P. No. 2, 91 Gif-sur-Yvette, France.
§Present address: University of Oxford, Keble Road, Oxford, England.

[1]D. J. Herndon, P. Soding, and R. J. Cashmore, Phys. Rev. D 11, 3165 (1975).
[2]A. H. Rosenfeld, D. J. Herndon, R. S. Longacre, R. J. Cashmore, and D. W. G. S. Leith, Phys. Lett. 55B, 486 (1975); L. R. Miller (Ph.D. thesis), Report No. LBL-38, Lawrence Berkeley Laboratory (unpublished); D. J. Herndon (Ph.D. thesis), Report No. LBL-554, Lawrence Berkeley Laboratory (unpublished).
[3]R. J. Cashmore, D. W. G. S. Leith, R. S. Longacre, and A. H. Rosenfeld, G. P. Gopal, R. A. Stevens, V. Tayler, and A. White, Report No. LBL-2634/SLAC-PUB-1387 (unpublished).
[4]D. J. Herndon, R. S. Longacre, L. R. Miller, R. J. Cashmore, and D. W. G. S. Leith, Phys. Rev. D 11, 3183 (1975).
[5]R. J. Cashmore, D. W. G. S. Leith, R. S. Longacre, and A. H. Rosenfeld, Nucl. Phys. 92, 37 (1975).
[6]R. S. Longacre, A. H. Rosenfeld, T. Lasinski, G. Smadja, R. J. Cashmore, and D. W. G. S. Leith, Phys. Lett. 55B, 415 (1975).
[7]H. H. Rosenbrock, Comput. J. 3, 175 (1960).
[8]G. Smadja, Orsay University of Paris, Ph.D. thesis, 1969, Appendix III, p. 89 and Sec. III, p. 31 (unpublished).
[9]P. Graves Morris, Nuovo Cimento 54, 818 (1968) (see especially p. 822).
[10]D. A. Jacobson, Nuovo Cimento 51A, 624 (1967) [see especially p. 628, Eq. (17)].
[11]J. M. Blatt and V. F. Weisskopf, *Theoretical Nuclear Physics* (Wiley, New York, 1956), p. 361.
[12]F. von Hippel and C. Quigg, Phys. Rev. D 5, 624 (1972).
[13]S. Almahed and C. Lovelace, Nucl. Phys. B40, 157 (1972).
[14]R. Ayed, P. Bareyre, and Y. Lemoigne, contributed paper to the XVIth International Conference on High Energy Physics, Chicago-Batavia, Ill., 1972 (unpublished).
[15]In our energy-independent fit, we had a complete set of $N\pi\pi$ data from 1310–1970 MeV except for a gap of data in the region 1510 to 1650 MeV.
[16]R. S. Longacre (Ph.D. thesis), Report No. LBL-948, Lawrence Berkeley Laboratory, 1973 (unpublished).
[17]K. T. R. Davis and M. Baranger, Ann. Phys. (N.Y.) 19, 383 (1962); C. J. Goebel and K. W. McVoy, Phys. Rev. 164, 1932 (1967).
[18]J. S. Ball *et al.*, Phys. Rev. D 7, 2789 (1973).
[19]P. Söding, Phys. Rev. D 12, 3762 (1975).
[20]Y. Lemoigne *et al.*, in *Baryon Resonances — 73*, proceedings of the Purdue Conference, edited by E. C. Fowler (Purdue Univ. Press, Lafayette, Indiana, 1973).
[21]E. Flaminio *et al.*, Report No. CERN/HERA 70-5, 1970 (unpublished).